FAILURE ANALYSIS OF TAPERED COMPOSITE STRUCTURES UNDER TENSILE LOADING

A THESIS SUBMITTED TO

THE GRADUATE SCHOOL OF NATURAL AND APPLIED SCIENCES

OF

MIDDLE EAST TECHNICAL UNIVERSITY

BY

OZAN ÇELİK

IN PARTIAL FULFILLMENT OF THE REQUIREMENTS

FOR

THE DEGREE OF MASTER OF SCIENCE

IN

MECHANICAL ENGINEERING

SEPTEMBER 2016

Approval of the thesis:

FAILURE ANALYSIS OF TAPERED COMPOSITE STRUCTURES UNDER TENSILE LOADING

submitted by **OZAN ÇELİK** in partial fulfillment of the requirements for the degree of **Master of Science in Mechanical Engineering Department, Middle East Technical University** by,

Prof. Dr. M. Gülbin Dural ÜNVER _____
Director, Graduate School of **Natural and Applied Sciences**

Prof. Dr. R. Tuna BALKAN _____
Head of Department, **Mechanical Engineering**

Prof. Dr. K. Levend PARNAS _____
Supervisor, **Mechanical Engineering Dept., TEDU**

Examining Committee Members:

Prof. Dr. Hakan İ. TARMAN _____
Mechanical Engineering Dept., METU

Prof. Dr. Levend PARNAS _____
Mechanical Engineering Dept., TED University

Assoc. Prof. Dr. Ergin TÖNÜK _____
Mechanical Engineering Dept., METU

Asst. Prof. Dr. Gökhan O. ÖZGEN _____
Mechanical Engineering Dept., METU

Prof. Dr. Mehmet Ali GÜLER _____
Mechanical Engineering Dept., TOBB ETU

Date:

I hereby declare that all information in this document has been obtained and presented in accordance with academic rules and ethical conduct. I also declare that, as required by these rules and conduct, I have fully cited and referenced all material and results that are not original to this work.

Name, Last name: Ozan ÇELİK

Signature:

ABSTRACT

FAILURE ANALYSIS OF TAPERED COMPOSITE STRUCTURES UNDER TENSILE LOADING

Çelik, Ozan

M. Sc., Department of Mechanical Engineering

Supervisor: Prof. Dr. K. Levend Parnas

September 2016, 97 pages

A three dimensional finite element modeling approach is used to evaluate the effects of preliminary design variables on the performance of tapered composite laminates under tensile loading. Hashin failure criteria combined with a progressive failure algorithm is used for in-plane failure mechanisms and cohesive zone method is used for out-of-plane failures. The modeling approach is validated by a comparison with experimental results from literature. The validated model is used to examine various design variables in terms of their effect on the ultimate tensile strength of the tapered laminate. Finite element models are created for several preliminary design variables and their effects are discussed.

Keywords: Tapered Composites, Delamination, Failure Criteria, Cohesive Zone Method, Progressive Failure Analysis, Finite Element Analysis

ÖZ

DEĞİŞKEN KESİTLİ KOMPOZİT YAPILARIN ÇEKME YÜKÜ ALTINDA HASAR ANALİZİ

Çelik, Ozan

Yüksek Lisans, Makina Mühendisliği Bölümü

Tez Yöneticisi: Prof. Dr. K. Levend Parnas

Eylül 2016, 97 Sayfa

Ön tasarım değişkenlerinin değişken kesitli kompozit yapıların çekme yükü altındaki performansına etkisinin araştırılması amacıyla üç boyutlu sonlu elemanlar ile modelleme yaklaşımı kullanılmıştır. Düzlem içi hasarlar için İlerlemeli Hasar Algoritması ile birlikte Hashin hasar kriterleri, düzlem dışı hasar modellemesi için ise Yapışkan Bölge Yöntemi kullanılmıştır. Modelleme yaklaşımı literatürden edinilmiş deneysel bir çalışma ile karşılaştırılarak doğrulanmıştır. Doğrulanmış modelleme yöntemi farklı tasarım değişkenlerinin değişken kesitli kompozit serimin çekme yükü altındaki kopma direncine etkisini belirlemek üzere kullanılmıştır. Pek çok farklı ön tasarım değişkeni için sonlu elemanlar modelleri oluşturulmuş ve bu değişkenlerin yarattığı değişimler tartışılmıştır.

Anahtar Kelimeler: Değişken Kesitli Kompozitler, Delaminasyon, Hasar Kriterleri, Yapışkan Bölge Yöntemi, İlerlemeli Hasar Analizi, Sonlu Elemanlar Analizi

ACKNOWLEDGEMENTS

I would like to express my deepest gratitude for my supervisor Prof. Dr. Levend Parnas for his guidance, advice, criticism and encouragement throughout the research.

I would also like to thank my parents Nilgün and Ahmet Çelik for their never-ending support, patience and love.

TABLE OF CONTENTS

LIST OF TABLES

LIST OF FIGURES

LIST OF SYMBOLS AND ABBREVIATIONS

Symbols

C_d	Damaged elasticity matrix
d_f	Fiber damage variable
d_m	Matrix damage variable
d_s	Shear damage variable
δ	Separation for cohesive elements
δ_{eq}	Equivalent displacement for in-plane failure
δ_m	Effective displacement for cohesive elements
E_i	Young's modulus
ε	Strain tensor
G_C	Critical strain energy release rate
G_{ij}	Shear modulus
l_{cz}	Cohesive zone length
l_e	Element length in the cohesive length
L^c	Characteristic length
M	Damage operator
M_c	Cohesive zone length estimation parameter
N_e	Element count in the cohesive length
v_{ij}	Poisson's ratio
S	Shear strength
σ	Normal stress tensor

σ_{eq}	Equivalent stress for in-plane failure
σ_{true}	True stress tensor
$\mathbf{t}$	Traction stress vector for cohesive elements
T_0	Undeformed thickness of cohesive elements
τ	Shear stress tensor
τ^0	Interfacial strength for cohesive elements
URX, URY, URZ	Rotational degrees of freedom in X, Y and Z directions
UX, UY, UZ	Translational degrees of freedom in X, Y and Z directions
X_T, X_C	Tensile and compressive strengths of a lamina in the longitudinal direction
Y_T, Y_C	Tensile and compressive strengths of a lamina in the first transverse direction
Z_T, Z_C	Tensile and compressive strengths of a lamina in the second transverse direction

Abbreviations

CZM	Cohesive zone method
FEM	Finite element method
PFA	Progressive failure analysis
SD	Staircased-dispersed drop configuration
SG	Staircased-grouped drop configuration
UD	Uni-directional

VCCT	Virtual crack closure technique
XFEM	Extended Finite Element Method

CHAPTER 1

INTRODUCTION

1.1 A General View

Advanced composite materials, with improvements in materials science, production technique and testing capabilities, have become a major preference in material selection for many applications due to their high modulus, strength and damage tolerance properties with minimum weight. Aerospace industry is such a field, continuously demanding improvements which reduce the weight of components used in the vehicles while maintaining the integrity and strength of them.

Laminated composites are widely used due to its availability and simplicity for manufacturing a wide range of geometries in terms of complexity. In this type of composites, laminae are stacked onto each other on a tooling surface and then cured with various methods to form the structure. Due to the complicated architecture of laminated composites, many failure mechanisms may play a role while the composite structure is in service. Therefore, multiple failure modes should be checked depending on the application area.

The main failure modes of composite laminates are mainly divided into two categories; in-plane and out-of-plane failures. In-plane failure, also called intralaminar failure, occur in the surfaces limited by the boundaries of each lamina. This type of failure includes matrix and fiber failures, both in tensile and compressive manner. Another failure mode is out-of-plane failure, which is the separation of stacked

laminae from each other. This phenomenon is named as delamination and considered as a very dangerous type of failure due to the fact that it is very hard to detect and catastrophic. Delamination also reduces the stiffness and load carrying capacity for bending and compressive loads. Moreover, as the delamination crack grows, load distribution in the part changes instantaneously, making it difficult to foresee the behavior of the structure.

Serious efforts have been made to accurately predict the failure mechanisms of composites for more than 60 years. As a result, many approaches and theories have been proposed in this field to predict both in-plane and out-of-plane failure phenomena in composites. From very conservative methods like first-ply-failure to complex models considering both in-plane and out-of-plane models are available with varying ranges of applicability and accuracy.

In rotary wing aircraft, many types of composite materials are used in the rotor section. Rotor blades are hybrid structures containing thick, thin or sandwich composites with combinations of different materials. However, the main load carrying member in a rotor blade is the spar, or equivalently a flexbeam, whose purpose is to resist centrifugal loads caused by the rotation of the blade and bending loads resulting from aerodynamic forces. Since the acting forces cause axial stresses in those structures, spars and flexbeams are mostly made of unidirectional (UD) plies. Additionally, to satisfy stiffness and mass constraints in different regions of a blade, changing the thickness of the spar or flexbeam is essential. The change in thickness is obtained by dropping plies off at different locations. As an example, plies in a rotor blade are dropped in the transition region, where a large thickness change in a short distance is desired and in the functional region, where dynamic performance and strength criteria are satisfied by tuning parameters such as stiffness or mass at different sections (Figure 1 and Figure 2). Scheme of a typical internal drop-off can be

seen in Figure 3. Laminates with drop-offs are called tapered laminates and this name is used in the rest of this text to refer to them. The drop-off regions are sources of stress singularity in tapered laminates and therefore, their effects should be carefully calculated to evaluate a safe design with high performance. In this study, the behavior of tapered laminates is investigated under tensile load, since this mode of loading is very dominant in rotor blades.

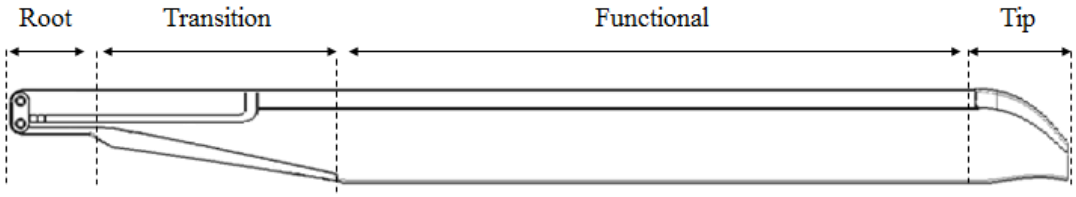

Figure 1. A typical rotor blade and root, transition, functional and tip regions

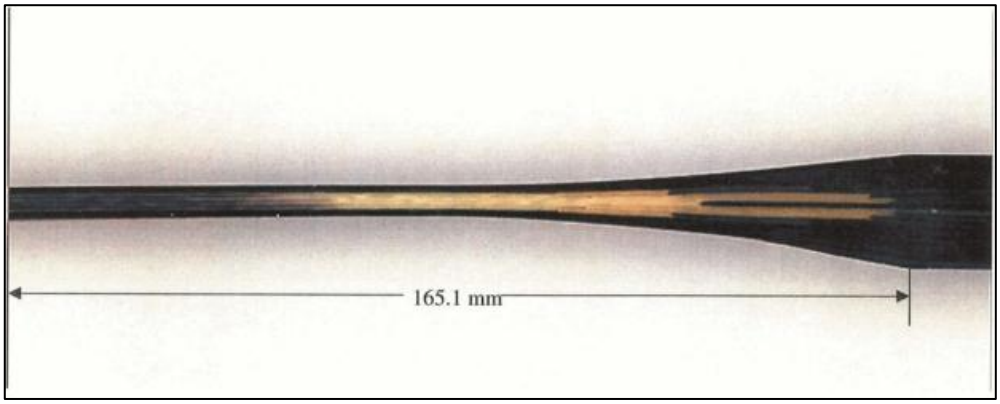

Figure 2. Carbon-glass hybrid flexbeam [1]

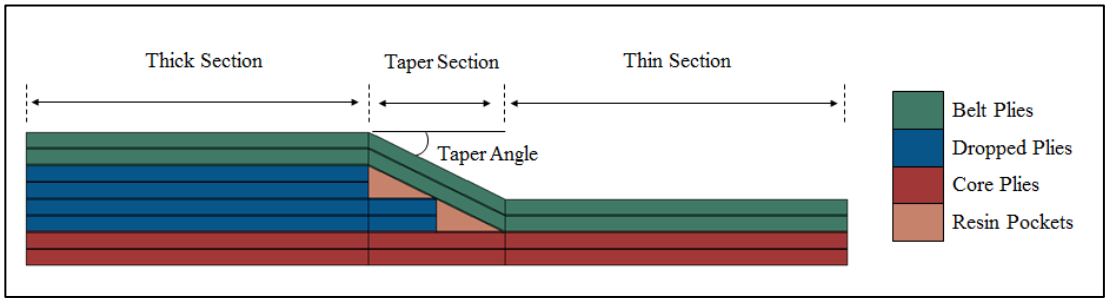

Figure 3. Schematic of a typical internal drop-off

1.2 Motivation

Currently in rotorcraft industry, durability and damage tolerance of composite parts are ensured by extensive testing in component level. Analytical methodologies for certification of such parts have not yet been in use. This situation is undesired because testing process is very time and source consuming. Also, preliminary design of tapered composite structures is mostly based on experience and design rule of thumbs. A methodology that will provide insight to designers by explaining the characteristic of the tapered structure until failure is demanded.

1.3 Objective

In this work, effects of several design variables on the ultimate tensile strength of a tapered laminate are investigated. The design variables are the drop configuration, the drop length, belt/core ply counts and dropped ply count at a drop station. The thick and thin side ply counts are constant. The failure behavior of the tapered laminate is described by two models representing the in-plane failure and delamination phenomena. Hashin failure theory [2] is used for in-plane damage initiation due to its accuracy level compared to its low requirement of material data and ease of

implementation. For the in-plane damage evolution, linear energy-based softening rules are applied. A detailed discussion of the various failure theories is given in the following chapters. Also, another key aspect of the failure analysis is predicting the initiation and evolution of the delamination cracks which are a result of interlaminar normal or shear stresses. The Cohesive Zone Method (CZM) is selected to simulate the delamination phenomenon due to its capability to predict the behavior of the crack from initiation up to failure, adjustability and ease of implementation. The CZM is investigated in a deeper manner in the following chapters. For the validation of the parametric study, experimental results from Samborsky et al. [3] are compared with the findings of the progressive failure analysis.

CHAPTER 2

LITERATURE SURVEY

2.1 Review of the Studies Related to Tapered Composites

With the increased use of tapered composites, several empirical and analytical studies have been conducted in the past decades. Researchers have been investigating tapered laminates from many aspects such as static strength, fatigue life and dynamic characteristics. Below are listed some previous work relevant to the subject of this thesis.

Hoa et al. [4] investigated the interlaminar stresses in unidirectional layers of glass-epoxy and graphite-epoxy. Due to computational restrictions, they used a submodeling scheme, in which interpolation of the node displacements from a coarse mesh is transferred to a finer mesh as a boundary condition. They compared finite element results with experiment results for glass-epoxy laminates and concluded to a consistency. However, interlaminar tensile stresses found by the finite element analysis changed with mesh refinement, representing a singularity. They did not use fracture mechanics concepts to overcome this problem, they only decided on an acceptable mesh size that agreed with the experimentally detected delamination failure.

Armanios and Parnas [5] constructed a two-dimensional analytical model to analyze a tapered laminate under tensile loading. Their modeling approach included two scales, global and local, namely. They estimated the total strain energy release rate in terms

of axial stress resultants and effective stiffness distribution by utilizing the global energy balance of the laminate. The output of their study also included the interlaminar stress distribution which was determined based on the basis equilibrium conditions and local stiffness variations at the ply drop locations. Their method showed an agreement with the finite element results of Salpekar et al [6] in terms of the trending behavior. Their approach does not intend to provide detailed information about a certain laminate but rather give insight for a general evaluation between candidate designs.

Curry et al. [7] investigated the effect of the count and orientation of the dropped plies on the tensile and compressive characteristics of glass-epoxy laminates. An experimental campaign with 37 specimens was conducted. All of the specimens had identical belt and core ply stacks but different dropped ply sequences. Test results showed that as the thickness of the dropped plies increases, ultimate strength for both tensile and compressive loading decreases due to the severity of the stiffness change. The specimens were analyzed for failure with finite element method, using both intralaminar and strength based interlaminar failure criteria. The analyses predicted the strength of the laminate lower than the experimental result.

Fish and Vizzini [8] produced four different kinds of taper geometries made of unidirectional glass/epoxy material to examine their performance under static and fatigue tensile loading. They determined the delamination onset loads of the specimens and the amount of bending stiffness they retain after delamination. They found that the structural integrity of a tapered structure can be increased by the selection of ply drop location and configuration judiciously. Their results also suggest that there is a trade-off between the delamination onset load and the bending stiffness retention. As the distance between the resin pockets closest to the thin section and the mid-plane decreases, the onset load increases and the retained amount of bending

stiffness decreases. The overlapped-dispersed configuration was found to be effective in terms of bending stiffness retention upon delamination fatigue life and stable delamination growth.

Wisnom et al. [9] designed, manufactured and tested glass and carbon laminates with different taper configurations. They observed that specimens reached net section tensile strength under static loading. When fatigue load is concerned, glass specimens again achieved net section strength, while the carbon specimens suffered a reduction in fatigue strength compared to net section strength. They found the most important parameter that affects the strength to be the count of plies dropped in a step. Another conclusion reached by them is that unidirectional drops are more susceptible to delamination when compared to dropped ±45-deg plies. Moreover, an analytical formula was used to predict the strength of the laminates and compared with test results. Satisfactory predictions were made.

Vizzini and Lee [10] used finite element models to determine the location of the onset of delamination and how the failure mechanism works. They modeled 3 different lay-up configurations with 3-dimensional finite elements. The choice of 3-dimensional elements is explained by the necessity to capture the taper-free edge interaction to properly investigate the phenomenon. Additionally, they investigated the effect of the thickness of the resin layers which he used to simulate the interface between the plies on the delamination paths. Results of the analyses have shown that maximum interlaminar stresses occur at the ply drop region, increasing with decreasing interface resin layer thickness. On the transverse direction, the effect of the free edges was clearly shown. A peak in the interlaminar stresses was observed on the stress-free edges. This effect could not be caught without 3-dimensional finite elements. Moreover, mode and extent of damage was tried to be captured by applying progressive failure to resin interface elements. Resin pocket failed prior to

delamination according to the results. Finally, interlaminar stress state around the ply drop-off was investigated with a model in which resin behaves as an elastic foundation and the plies are rigid. It is concluded that interlaminar stress state cannot be appropriately explained by how the belt plies are aligned. The way delamination is handled in this paper does not include the stress singularity at the front of the propagating crack or the internal stress-free boundary.

Carrella-Payan et al. [11] performed a characterization study on asymmetrically tapered composite laminates. The study included analytical calculations, finite element simulation and experiments of asymmetrically tapered carbon-epoxy specimens. Analytical formulation for delamination proposed by Petrossian and Wisnom [12] was used to predict a delamination onset load, which gave an over-predicting result since it only accounted for a delamination in the thick section. However, the finite element model used could predict a similar behavior to that observed in the experiments. They used VCCT formulation to simulate delamination growth. They prepared two finite element models; the first one is an idealized geometry of the drop-off section, whereas the second one is a detailed one based on images of the real specimen. They concluded that the idealized models should be preferred since they gave conservative results and were easier to implement.

2.2 Review of the Cohesive Zone Method (CZM)

Delamination is a major failure mode for composites which causes insidious and sudden degradation of the stiffness and strength properties of the laminate. Therefore, its investigation plays a crucial role in designing safe and reliable parts. The CZM is an up-to-date and flexible method to predict delamination behavior. In this section, a general review of the method and the theoretical background beneath it are given.

Significant work on the CZM dates back to the work of Barenblatt [13] and Dugdale [14], investigating the formation of cracks in brittle and ductile materials, respectively. Later, Hillerborg et al. [15] applied the CZM using the finite element method by modeling a linear softening behavior with equivalent nodal forces. Since then, many different cohesive surface or solid finite elements have been proposed. Now, the CZM is a built-in option for modeling crack initiation and growth in many commercial finite element solvers.

The CZM assumes a cohesive zone ahead of the crack-tip to predict the onset and growth of the crack, which can be seen in Figure 4. This cohesive zone acts with a softening plasticity behavior. The CZM creates a connection between the microstructural failure mechanisms and macroscopic structures governing bulk deformations. Therefore, the parameters that characterize a cohesive model are the mechanical properties of the bulk material, a crack initiation state and a function describing crack evolution. These parameters are mathematically formulated in constitutive models for cohesive elements, namely traction-separation laws. In these models, traction on the cohesive element is related to the opening of the crack in the corresponding mode (Mode I, II or III). Crack opening modes can be seen in Figure 5. Up to damage initiation, the cohesive element deforms as a bulk material. The point where damage initiates is denoted with T, namely the interfacial strength. δ^0 denotes the critical opening for damage initiation. δ^{fail} is the separation at complete failure and the area under the traction-separation curve represents the critical strain energy release rate G_c. The shape of the traction-separation curve can be in many different forms as in Figure 6.

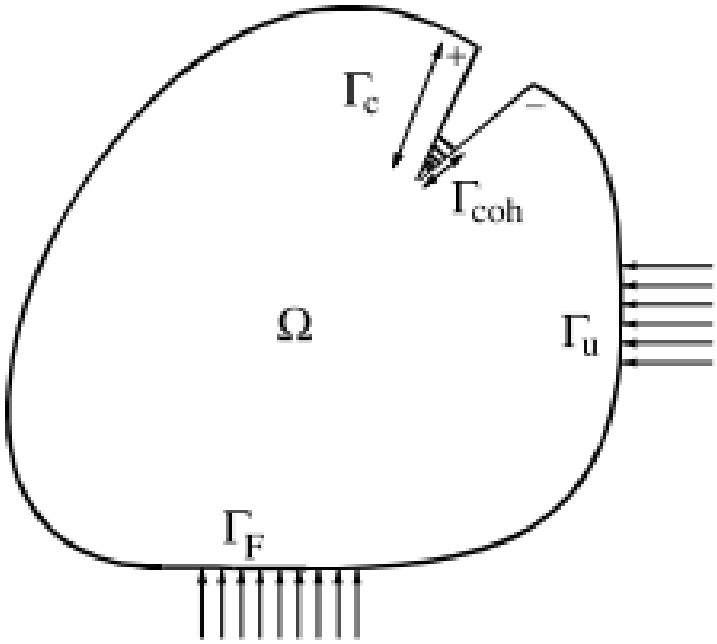

Figure 4. Crack growth in a continuous body Ω and the cohesive zone of the crack [16]

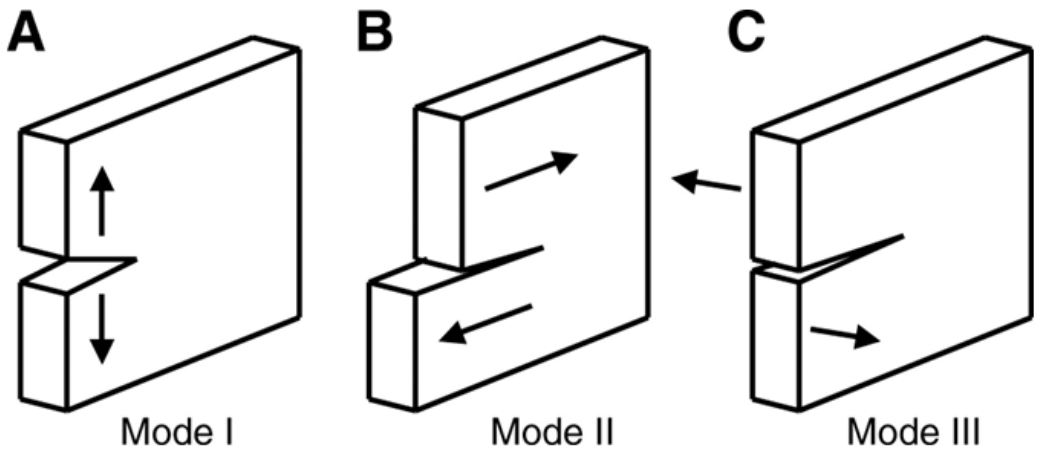

Figure 5. Crack opening modes

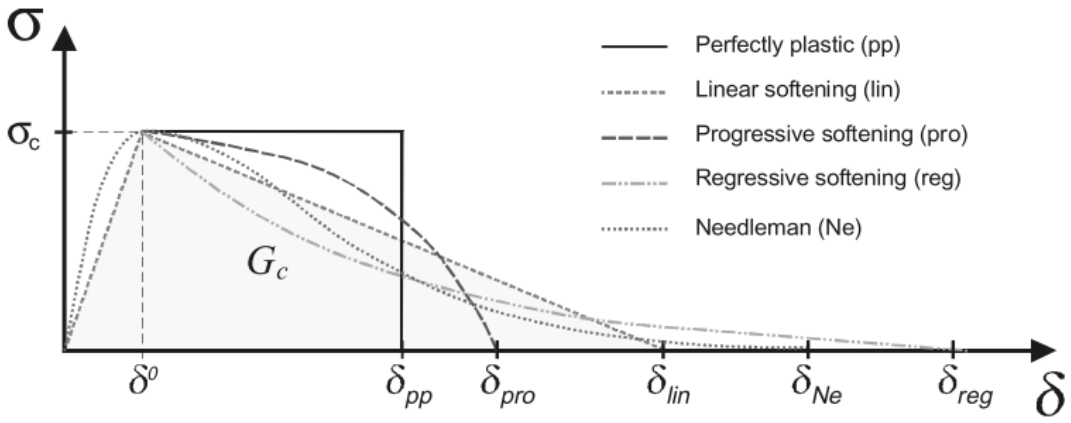

Figure 6. Different traction-separation curves [17]

The CZM is implemented in a finite element model by adding cohesive zone elements along potential crack growth paths as shown in Figure 7. As the opening stresses increase on cohesive elements, damaged cohesive elements simulate the initiation and growth of cracks. Cohesive elements start opening when the tractions on them reach the respective critical value and softening begins. As the traction increases, faces of the cohesive elements separate according to the traction-separation law defined.

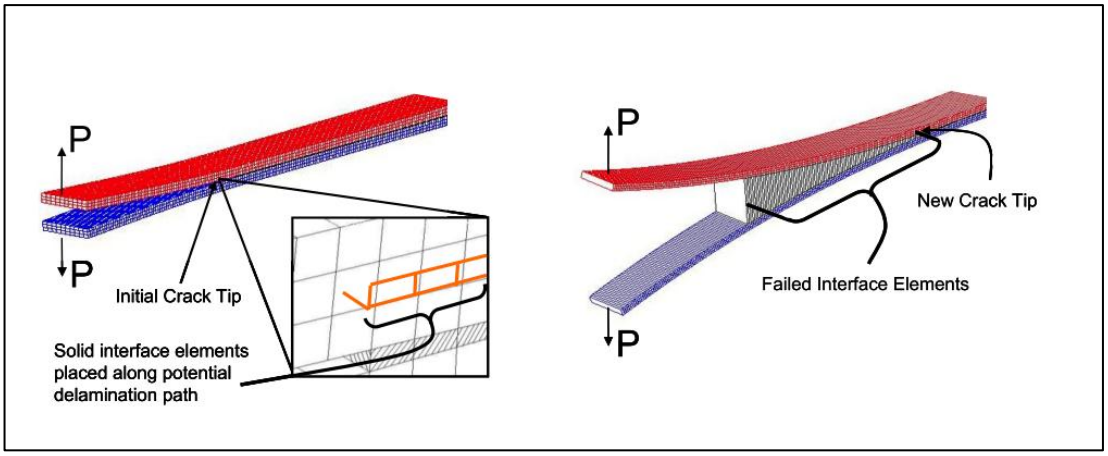

Figure 7. Undamaged and damaged cohesive elements on a DCB model [18]

Despite its advantages, the CZM brings some numerical difficulties when implemented to finite element simulations. Requirement of excessively refined meshes, convergence problems caused by the implementation of the softening behavior and a correct description of the cohesive layer are the main issues. Several studies such as Falk et al. [19], Davila et al. [20], Turon et al. [21][16] and Harper & Hallett [18] have been conducted on the parameters affecting the behavior of cohesive elements. Turon et al. emphasize the stiffness and the size of the cohesive zone elements as important factors affecting the reliability of a FEM simulation including crack initiation and growth. The stiffness of the cohesive elements must be small enough that they do not affect the global response of the structure in terms of stiffness and the size of them must be smaller than the cohesive length, defined by the distance between the point where maximum traction occurs and the crack tip, to capture the crack behavior properly. The cohesive length is found with the following relationship:

$$l_{cz} = M_c E \frac{G_c}{(\tau^0)^2} \tag{2-1}$$

where l_{cz} is the cohesive zone length, E is the Young's modulus of the material, G_c is the critical energy release rate, τ^0 is the interfacial strength and M_c is a parameter depending on the model for cohesive zone length estimation. The value of M is taken as 0.21, 0.31, 0.4, 0.88 and 1 by Hui et al. [22], Irwin [23], Dugdale [14], Rice [24] and Hillerborg et al. [15], respectively. With this definition of the cohesive length, minimum element size can be found by defining an element number per cohesive length. 3 elements in the cohesive length is advised in [21] to properly capture the crack propagation, which leads to the following formula:

$$N_e = \frac{l_{cz}}{l_e} \geq 3 \tag{2-2}$$

where N_e is the number of elements in the cohesive zone and l_e is the length of the cohesive zone element. However, this methodology may lead to very small element requirements since the cohesive length is in the order of 1 mm to capture the delamination in a double cantilever beam (DCB) specimen as stated in [20]. To

overcome this problem and create computationally feasible models, Turon developed a methodology using the findings of Alfano and Crisfield [25], which state that variations in the interfacial strength of the cohesive elements does not affect the predicted results significantly . The proposal of Turon allows a larger size of cohesive elements by lengthening the cohesive zone. The cohesive zone is lengthened by setting a lower interfacial strength, which is determined by the desired number of elements in the cohesive zone by the following formula:

$$\bar{\tau}^0 = \sqrt{\frac{EG_c}{N_e^0 l_e}} \tag{2-3}$$

where N_e^0 is the desired element count in the cohesive zone and $\bar{\tau}^0$ is the corresponding interfacial strength value. Finally, the appropriate interfacial strength is determined by:

$$T = min\left\{\tau^0, \bar{\tau}^0\right\} \tag{2-4}$$

These equations are useful for obtaining an efficient, yet accurate finite element model and will be used in the finite element models of tapered laminates in the latter chapters.

2.3 Review of In-Plane Failure Criteria for Composite Materials

The ability to accurately predict how the damage occurs in a composite structure is very essential to designers. However, the complex nature of the composites makes it difficult to connect the microstructural properties of a laminate with its global behavior. Moreover, the formulation used to describe the failure phenomenon of composites should be composed of parameters that can be extracted from real-life tests or observations. The search for a proper explanation for the failure of composite materials has been active for few decades. Many theories have been proposed and this topic is still under investigation densely.

Apart from delamination, in-plane damage in composites is observed in the following forms: fiber tension, fiber compression, matrix tension and matrix compression. These modes of failure can be described as follows: ([26] and [27])

Fiber tensile failure occurs when the fibers in a composite structure are damaged so that there are not enough of them to bare the loads applied. This type of failure usually results in catastrophic damage in the structure. The load carrying capacity of the structure decreases sharply, releasing a large amount of energy.

Fiber compressive failure is in close relationship with the resin shear behavior and defects in the structure such as voids and misalignments in the fiber placement. Fiber micro-buckling, matrix shear or fiber compressive failures are the consequence of this type of failure and can be observed in the form of kinking bands.

Matrix tensile failure is often a result of normal and shear stresses on a critical fracture plane in the transverse tension direction. Fibers may split due to the breakage of the matrix material linking them to the rest of the structure.

Matrix compressive failure is mostly related to the shear stresses in the matrix material. The fact that failure surfaces make an angle with the loading direction is an evidence of this phenomenon.

Figure 8 shows the failure modes mentioned above schematically.

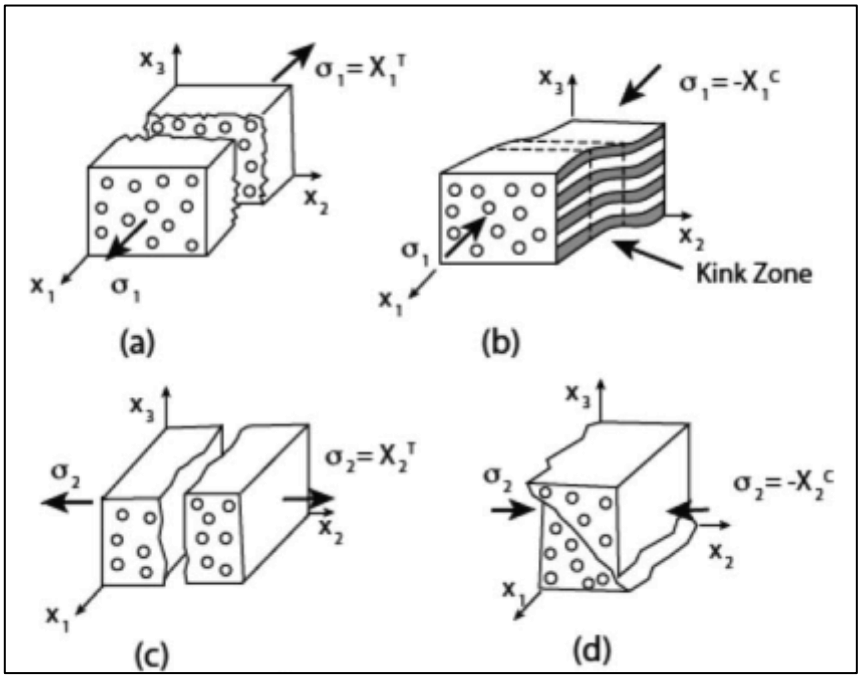

Figure 8. In-plane failure modes of composites a) Fiber tensile b) Fiber compressive c) Matrix tensile d) Matrix compressive [28]

As in the delamination mode, in-plane damage in composites is characterized by the onset and progression since the types of damage mentioned above may not immediately result in complete failure of the structure due to the complex nature of composites. The accumulation of a combination of these damage types lead to the ultimate failure, preceded by a loss of performance throughout loading. The ability to accurately predict the whole process up to failure is important for the assessment of the behavior of the structure.

Present failure criteria claim to capture damage only at ply-level. This means that a criterion which explains the behavior of a whole laminate under a certain load case is not available. In-plane damage initiation in a ply is mostly characterized by methodologies based on strength approaches. In some proposals, the strength concepts are extended with fracture mechanics concepts, such as the toughness ratio. In- plane

failure criteria for composites can be classified into two groups based on how they approach to the stress interaction: non-interactive and interactive failure criteria.

Non-interactive failure criteria do not consider the interactions between stresses to assess failure. The stresses cause failure only when they exceed the material strength in the corresponding direction. The contribution of different stresses in different directions is neglected in this type of failure criteria. Maximum stress and maximum strain criteria are examples of non-interactive theories that are commonly used. These theories are mostly applicable to brittle failure and to the cases where stress interactions do not have significant importance.

Table 1. Maximum Stress and Maximum Strain Criteria

Maximum Stress	**Maximum Strain**
For fiber failure: $\sigma_1 \geq X_T \; if \; \sigma_1 > 0$ $\lvert\sigma_1\rvert \geq X_C \; if \; \sigma_1 < 0$ For matrix failure: $\sigma_2 \geq Y_T \; if \; \sigma_2 > 0$ $\lvert\sigma_2\rvert \geq Y_C \; if \; \sigma_2 < 0$ For shear failure: $\lvert\sigma_{12}\rvert \geq S$	For fiber failure: $\varepsilon_1 \geq \varepsilon_{1_T} \; if \; \varepsilon_1 > 0$ $\lvert\varepsilon_1\rvert \geq \varepsilon_{1_C} \; if \; \varepsilon_1 < 0$ For matrix failure: $\varepsilon_2 \geq \varepsilon_{2_T} \; if \; \varepsilon_2 > 0$ $\lvert\varepsilon_2\rvert \geq \varepsilon_{2_C} \; if \; \varepsilon_2 < 0$ For shear failure: $\lvert\varepsilon_{12}\rvert \geq \varepsilon_{12}{}^{u}$

Interactive failure criteria, however, take the interaction between stresses or strains on a lamina into account to predict the onset of damage. More than one component of stress or strain may cause damage in a direction. In this type of criteria, some researchers have proposed criteria which do not distinguish the failure modes in a

lamina such as fiber or matrix failure. These so-called "fully interactive" criteria predict the failure of the whole ply using all the strength allowables of the materials to define a failure surface. Tsai-Wu criterion [29] is a commonly used example of this type of criteria. Despite the fact that these criteria are criticized for being unlinked with physical phenomena which play role in the damage process, they are widely available in software packages and used in industry due to the reasonable accuracy they provide when compared to the criteria based on different failure modes and simple implementation.

Table 2. Tsai-Wu Failure Criterion

Tsai-Wu Criterion
For ply failure: $$\left(\frac{1}{X_T}-\frac{1}{X_C}\right)\sigma_1+\left(\frac{1}{Y_T}-\frac{1}{Y_C}\right)\sigma_2+\frac{\sigma_1^2}{X_TX_C}+\frac{\sigma_2^2}{Y_TY_C}+\left(\frac{\tau_{12}}{S_{12}}\right)^2+2f_{12}\sigma_1\sigma_2\geq 1$$ $$f_{12}=-\frac{1}{2}\sqrt{\frac{1}{X_TX_CY_TY_C}}\ ,when\ not\ experimentally\ determined$$

Recent failure criteria consider different failure modes and the effects of interactions between stresses. The damage mechanisms mentioned above, fiber tension-compression, matrix tension-compression, are all modeled separately and have corresponding indices that indicate the failure in the corresponding mode. The interpretation of transverse tensile and shear strength may differ in this type of failure criteria. While a significant amount of theories use the unidirectional strengths of laminae, some criteria take into account the in-situ strength values. It is assumed by the in-situ strength concept that the plies have higher transverse and shear strength when they carry loads with adjacent plies with different orientations clustered together

than they have in a unidirectional laminate. Hashin [2] proposed a group of criteria formulated for different failure modes. This criteria has gained significant acceptance due to its success in predicting failure envelopes in reasonable accuracy and requirement of material properties that can be obtained via standard test procedures.

Table 3. Hashin Damage Initiation Criteria

Hashin Damage Initiation Criteria
Fiber Tension ($\sigma_{11} > 0$): $$F_f^t = \left(\frac{\sigma_{11}}{X_T}\right)^2 + \left(\frac{\tau_{12}}{S_L}\right)^2 \geq 1$$
Fiber Compression ($\sigma_{11} < 0$): $$F_f^c = \left(\frac{\sigma_{11}}{X_C}\right)^2 \geq 1$$
Matrix Tension ($\sigma_{22} > 0$): $$F_m^t = \left(\frac{\sigma_{22}}{Y_T}\right)^2 + \left(\frac{\tau_{12}}{S_L}\right)^2 \geq 1$$
Matrix Compression ($\sigma_{22} < 0$): $$F_f^t = \left(\frac{\sigma_{22}}{2S_T}\right)^2 + \left[\left(\frac{Y_C}{2S_T}\right)^2 - 1\right]\frac{\sigma_{22}}{Y_C} + \left(\frac{\tau_{12}}{S_L}\right)^2 \geq 1$$

Damage initiation criteria are used to predict the stress state at which a ply starts being damaged, meaning that the failure of the whole structure is not determined by them. To simulate the failure behavior of the laminate, progressive damage methodology is successfully applied by many researchers to many cases as in [30]. In this procedure, whenever a failure initiation criterion is satisfied at a load increment, stiffness of the material related to the failure mode is reduced. This decrease in stiffness simulates the lessening load carrying capacity of the structure as the damage accumulates. The complete failure of the structure is determined by introducing an independent

condition. There is no consensus over how the final failure of a laminate is defined, since it varies depending on the application and load case. Fiber breakage or delamination are usually considered as indicators of the final failure. In this study, the point where a sharp decrease at load on the load-displacement curve of the laminate is observed is considered to be the complete failure of the structure. A typical load-displacement curve can be seen in Figure 9. The progressive failure algorithm is presented in Figure 10.

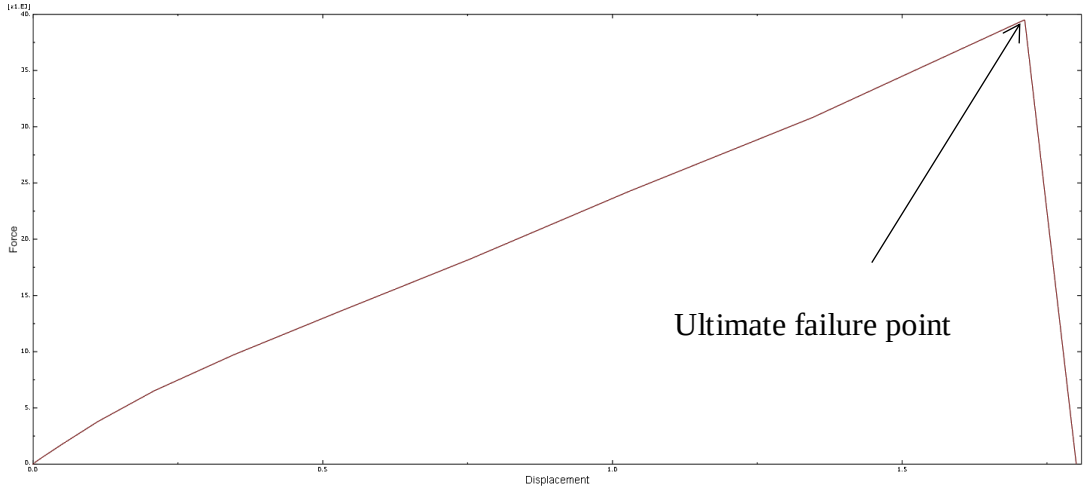

Figure 9. A typical load displacement curve for PFA

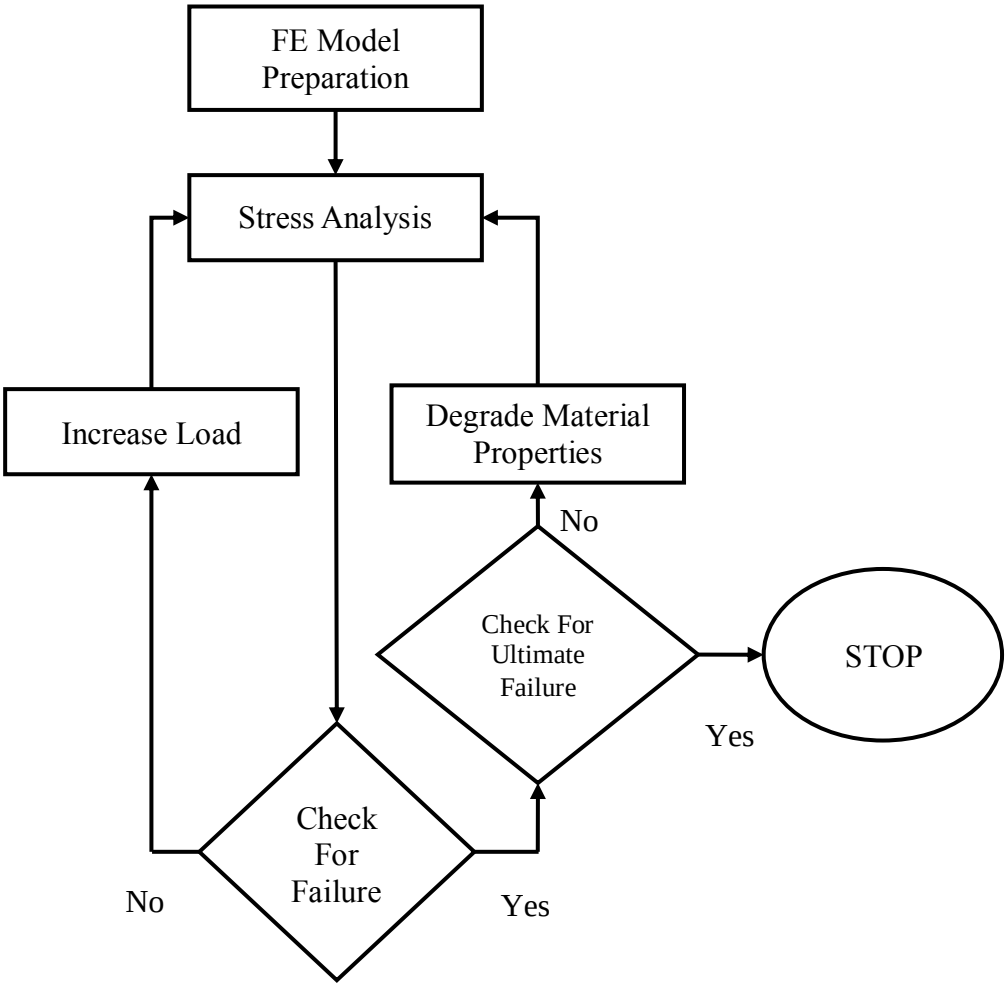

Figure 10. Progressive failure algorithm

CHAPTER 3

DESCRIPTION OF THE FE MODELING TECHNIQUE AND COMPARISON WITH A BENCHMARK STUDY

3.1 Validation Method

To observe the damage occurring in the composite structure during loading and evaluate the strength of the laminate, detailed finite element models have been created. Progressive failure algorithm has been applied to the models for the in-plane failures and cohesive zone elements have been utilized to simulate delamination. To validate the simulations, experimental data generated by Samborsky et al. [3] have been used to validate the finite element models. This study is selected since the author provided the initial failure mode of the tapered specimen. First, a finite element model to represent a flat test coupon with $[\pm 45/0_8/\pm 45]$ laminate is modeled. After the adequacy of the model to estimate the strength of the flat coupon is shown, a detailed 3-dimensional model of a $[\pm 45/0_2^*/0_9/\ 0_2^*/\pm 45]$ laminate, where the superscript '*' indicates the dropped plies is validated by the corresponding experimental data. In the experimental work, specimens were axially loaded with tensile load up to ultimate failure. Abaqus finite element package is used for analyses.

3.2 Implementation of In-Plane Failure Modes

Hashin failure criteria is used for in-plane damage initiation and linear, energy-based damage evolution is assumed. Detailed form of the Hashin criteria is given in Table 3. "σ" and "τ" which are mentioned in the initiation criteria are the effective normal and shear stress tensors, respectively. The effective stress tensors are computed from:

$$\sigma = M\sigma_{true} \tag{3-1}$$

where σ_{true} is the stress tensor for undamaged configuration and M is the damage operator:

$$M = \begin{bmatrix} \frac{1}{(1-d_f)} & 0 & 0 \\ 0 & \frac{1}{(1-d_m)} & 0 \\ 0 & 0 & \frac{1}{(1-d_s)} \end{bmatrix} \tag{3-2}$$

where d_f, d_m and d_s are internal (damage) variables that characterize fiber, matrix, and shear damage, which are derived from damage variables d_f^t, d_f^c, d_m^t and d_m^c, corresponding to the four modes previously discussed, as follows:

$$d_f = \begin{cases} d_f^t \; if \; \sigma_{11} \geq 0 \\ d_f^c \; if \; \sigma_{11} \leq 0 \end{cases} \tag{3-3}$$

$$d_m = \begin{cases} d_m^t \; if \; \sigma_{22} \geq 0 \\ d_m^c \; if \; \sigma_{22} \leq 0 \end{cases} \tag{3-4}$$

$$d_s = 1 - (1-d_f^t)(1-d_f^c)(1-d_m^t)(1-d_m^c) \tag{3-5}$$

M is equal to the identity matrix before any damage occurs. Therefore, true stress and effective stress tensors are equal to each other. Once a failure mode is activated, damage evolution takes place with a decrease in the stiffness of the composite material. The constitutive relation for a damaged material is:

$$\sigma = C_d \varepsilon \tag{3-6}$$

where ε is the strain tensor and C_d is the damaged elasticity matrix, which is in the following form:

$$C_d = \frac{1}{D}\begin{bmatrix} (1-d_f)E_1 & (1-d_f)(1-d_m)\nu_{21}E_1 & 0 \\ (1-d_f)(1-d_m)\nu_{12}E_2 & (1-d_m)E_2 & 0 \\ 0 & 0 & (1-d_s)GD \end{bmatrix} \tag{3-7}$$

where $D = 1 - (1 - d_f)(1 - d_m)\nu_{12}\nu_{21}$, E_1 and E_2 are Young's modulus in the longitudinal and transverse directions, respectively, G is the shear modulus and ν_{12} and ν_{21} are Poisson's ratios. To decrease mesh dependency during material softening, a characteristic length is included into the formulation in Abaqus software. The damage variable evolves such that a stress-displacement relation is established as shown in Figure 11 for each failure mode.

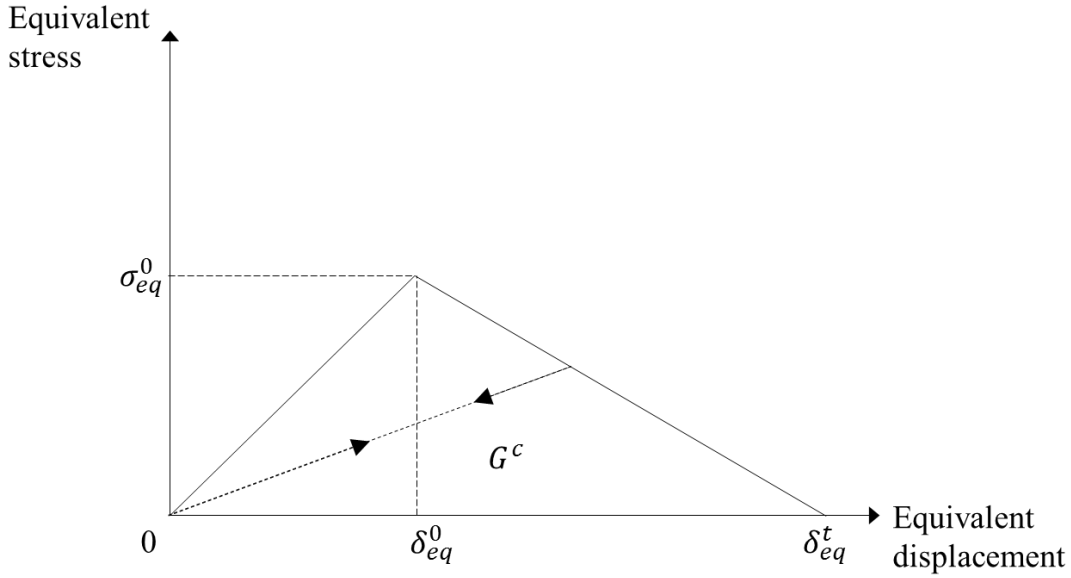

Figure 11. Equivalent stress-displacement curve for in-plane damage evolution

The positive slope of the stress-displacement curve prior to damage initiation corresponds to linear elastic material behavior; the negative slope after damage initiation is achieved by evolution of the respective damage variables according to the equations shown below.

Fiber tension $(\boldsymbol{\sigma_{11} \geq 0})$:

$$\delta_{eq}^{ft} = L^c \sqrt{\langle \varepsilon_{11} \rangle^2 + \varepsilon_{12}^2} \tag{3-8}$$

$$\sigma_{eq}^{ft} = \frac{\langle \sigma_{11} \rangle \langle \varepsilon_{11} \rangle + \tau_{12} \varepsilon_{12}}{\delta_{eq}^{ft} / L^c} \tag{3-9}$$

Fiber compression ($\boldsymbol{\sigma_{11} < 0}$):

$$\delta_{eq}^{fc} = L^c \langle -\varepsilon_{11} \rangle \tag{3-10}$$

$$\sigma_{eq}^{fc} = \frac{\langle \sigma_{11} \rangle \langle \varepsilon_{11} \rangle}{\delta_{eq}^{fc} / L^c} \tag{3-11}$$

Matrix tension($\boldsymbol{\sigma_{22} \geq 0}$):

$$\delta_{eq}^{mt} = L^c \sqrt{\langle \varepsilon_{22} \rangle^2 + \varepsilon_{12}^2} \tag{3-12}$$

$$\sigma_{eq}^{mt} = \frac{\langle \sigma_{22} \rangle \langle \varepsilon_{22} \rangle + \tau_{12} \varepsilon_{12}}{\delta_{eq}^{mt} / L^c} \tag{3-13}$$

Matrix compression($\boldsymbol{\sigma_{22} < 0}$):

$$\delta_{eq}^{mc} = L^c \sqrt{\langle -\varepsilon_{22} \rangle^2 + \varepsilon_{12}^2} \tag{3-14}$$

$$\sigma_{eq}^{mc} = \frac{\langle -\sigma_{22} \rangle \langle -\varepsilon_{22} \rangle + \tau_{12} \varepsilon_{12}}{\delta_{eq}^{mc} / L^c} \tag{3-15}$$

L^c is the characteristic length which depends on the element geometry and formulation. For linear elements, it is a typical length of a line across an element [31]. The symbol "⟨ ⟩" in the equations above represents the Macaulay bracket operator, which is defined for every $\alpha \in R$ as $\langle \alpha \rangle = (\alpha + |\alpha|)/2$.

After damage initiation (i.e., $\delta_{eq} \geq \delta_{eq}^0$) for the behavior shown in Figure 11, the damage variable for a particular mode is given by the following expression:

$$d = \frac{\delta_{eq}^f (\delta_{eq} - \delta_{eq}^0)}{\delta_{eq} (\delta_{eq}^f - \delta_{eq}^0)} \tag{3-16}$$

where δ_{eq}^0 is the initial equivalent displacement at which the initiation criterion for that mode was met and δ_{eq}^f is the displacement at which the material is completely

damaged in this failure mode. δ_{eq}^{0} is determined by the elastic stiffness and strength parameters of the material and δ_{eq}^{f} for each failure mode is determined such that the area under the triangular curve (the energy dissipated due to failure) in Figure 11 is equal to the respective fracture energy G^{c} defined by the user. An element is deleted from mesh when a damage variable associated with fiber failure modes (tensile or compressive) reaches unity at integration points. Deleted elements no longer carry any amount of load in any direction.

3.3 Implementation of Out-Of-Plane Failure Modes

The behavior of the cohesive elements between the plies is modeled with the bilinear traction-separation law, which is shown in Figure 12.

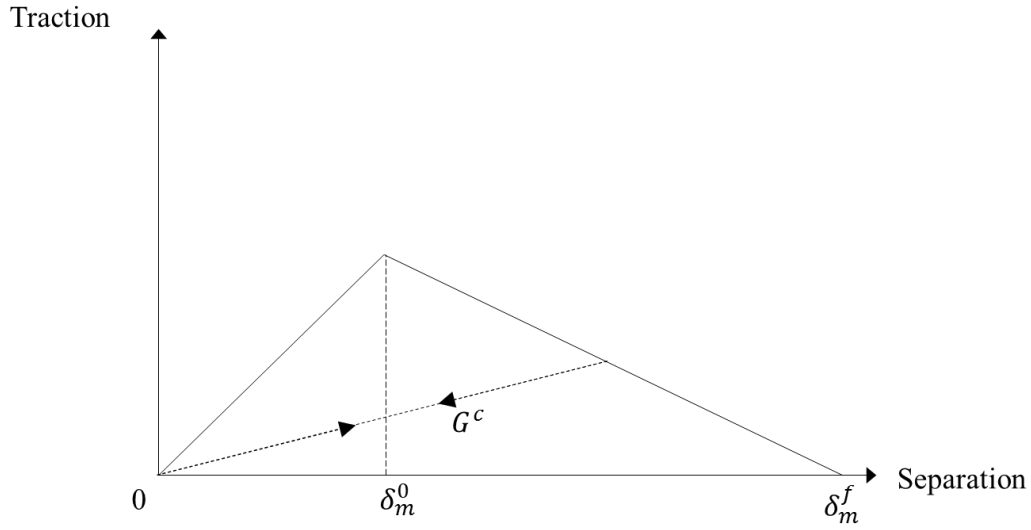

Figure 12. Bilinear traction-separation law

This model assumes initially linear elastic behavior followed by the initiation and evolution of damage. The elastic behavior is written in terms of an elastic constitutive

matrix that relates the nominal stresses to the nominal strains across the interface. The nominal stresses are the force components divided by the original area at each integration point, while the nominal strains are the separations divided by the original thickness at each integration point. The nominal traction stress vector, $\mathbf{t}$, consists of three components: t_n, t_s and t_t , which represent the normal (along the local 3-direction) and the two shear tractions (along the local 1- and 2-directions), respectively. The local directions of a cohesive element are shown in Figure 13..

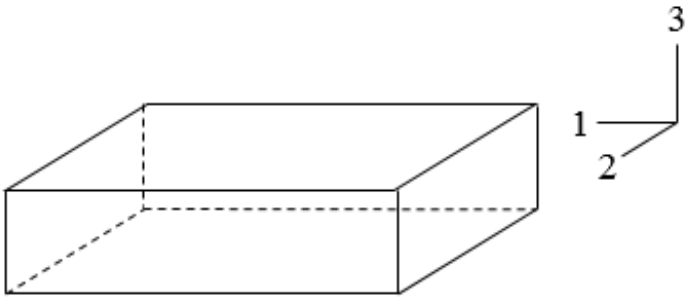

Figure 13. Local directions of a cohesive element

The corresponding separations are denoted by δ_n, δ_s and δ_t. T_0 representing the original thickness of the cohesive element, the nominal strains can be defined as:

$$\begin{aligned} \varepsilon_n &= \frac{\delta_n}{T_0} \\ \varepsilon_s &= \frac{\delta_s}{T_0} \\ \varepsilon_t &= \frac{\delta_t}{T_0} \end{aligned} \tag{3-17}$$

With these definitions, the elastic behavior of the cohesive elements can be written as:

$$\mathbf{t} = \begin{bmatrix} t_n \\ t_s \\ t_t \end{bmatrix} = \begin{bmatrix} E_{nn} & E_{ns} & E_{nt} \\ E_{ns} & E_{ss} & E_{st} \\ E_{nt} & E_{st} & E_{tt} \end{bmatrix} \begin{bmatrix} \varepsilon_n \\ \varepsilon_s \\ \varepsilon_t \end{bmatrix} = \mathbf{E}\varepsilon \tag{3-18}$$

Damage initiates when quadratic nominal stress criterion is satisfied. The criterion is represented in the following equation:

$$\left\{\frac{\langle t_n \rangle}{t_n^0}\right\}^2 + \left\{\frac{t_s}{t_s^0}\right\}^2 + \left\{\frac{t_t}{t_t^0}\right\}^2 = 1 \tag{3-19}$$

where t_n^0, t_s^0 and t_t^0 are the peak values of the nominal stress when the deformation is either purely normal to the interface or purely in the first or the second shear direction, respectively.

Following damage initiation, damage evolution is represented in terms of a scalar variable *D*. *D* is a measure of the overall damage done by the combination of normal and shear tractions. The stress components of the traction-separation model are affected by the damage parameter as follows:

$$t_n = \begin{cases} (1-D)\bar{t_n}, \bar{t_n} \geq 0 \\ \bar{t_n}, \bar{t_n} < 0 \ (no\ damage\ under\ compressive\ stresses) \end{cases}$$
$$t_s = (1-D)\bar{t_s} \tag{3-20}$$
$$t_t = (1-D)\bar{t_t}$$

where $\bar{t_n}$, $\bar{t_s}$ and $\bar{t_t}$ are the stress components predicted by the elastic traction-separation behavior for the current strains without damage. Cohesive elements completely fail when *D*=1.

To describe the evolution of damage under a combination of normal and shear deformation across the interface, an effective displacement proposed by Camanho and Davila [32] is useful. The following equation represents the effective displacement:

$$\delta_m = \sqrt{\langle \delta_n \rangle^2 + \delta_s^2 + \delta_t^2} \tag{3-21}$$

The effective displacement is used since the relative proportions of normal and shear deformations quantify the damage on the cohesive element. This method of computing the damage is called the mixed-mode definition. Figure 14 is a schematic representation of the dependence of damage initiation and evolution on the mode mix,

for a traction-separation response with isotropic shear behavior. The figure shows the traction on the vertical axis and the magnitudes of the normal and the shear separations along the two horizontal axes. Shear separation is shown as $\boldsymbol{\tau} = \sqrt{t_s^2 + t_t^2}$. The unshaded triangles in the two vertical coordinate planes represent the response under pure normal and pure shear deformation, respectively. All intermediate vertical planes (that contain the vertical axis) represent the damage response under mixed mode conditions with different mode mixes.

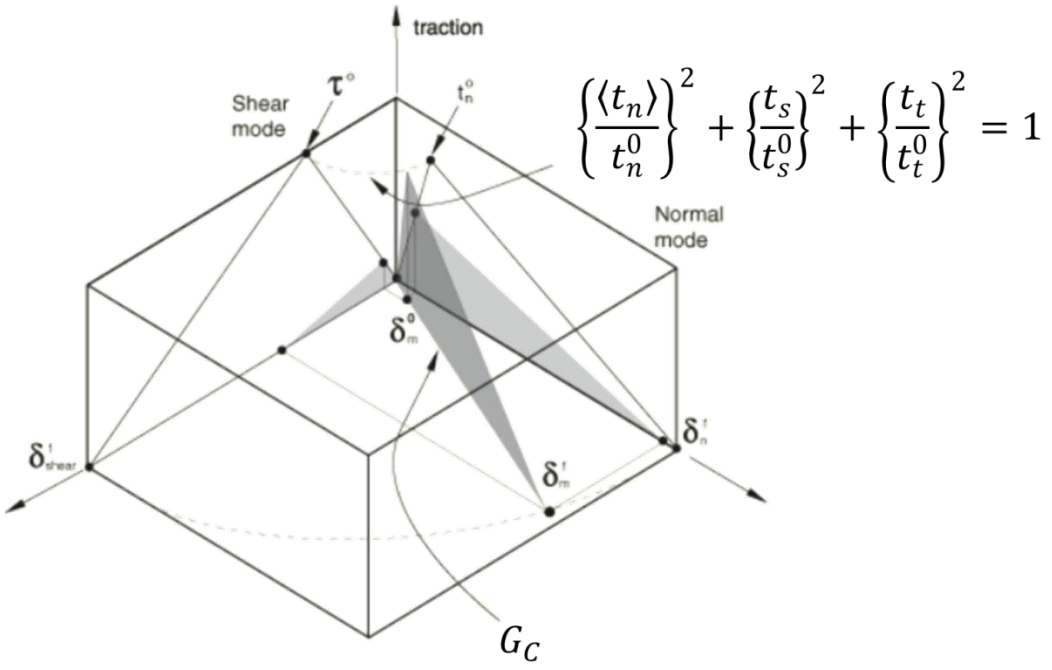

Figure 14. Damage response under mixed mode conditions with different mode mixes [31]

The linear softening model is accomplished by the damage variable *D* which is calculated as follows:

$$D = \frac{\delta_m^f(\delta_m^{max} - \delta_m^0)}{\delta_m^{max}(\delta_m^f - \delta_m^0)} \tag{3-22}$$

where δ_m^{max} is the maximum value of the effective displacement attained during the loading history, δ_m^0 is the effective displacement at the point where damage starts and δ_m^f is the effective displacement at the point where the cohesive element completely fails as shown in Figure 12.

3.4 Flat Plate Model

The flat plate is a rectangular-shaped, 240x25mm laminate with a [±45/0_8/±45] lay-up. 0 degree plies are made of carbon fibers and ±45 degree plies are made of E-glass 2-D woven system, while the resin system of the laminae is epoxy. 3.175-mm thick G10 tabs were used to provide proper gripping and prevent premature failures during the test. The details of the geometry are presented in Figure 15. Material properties for carbon and woven E-glass used in the study are given in Table 4. The model created is shown in Figure 16. A quarter model of the coupon is used with appropriate symmetry conditions. Both E-Glass and carbon layers are meshed with SC8R continuum shell elements. 0.05mm-thick cohesive layers are added between the plies in the active region and meshed with COH3D8 linear hexahedron cohesive elements. Explicit solution procedure is used in the analysis since a more efficient solving process can be obtained for problems with progressive failure algorithm.

Table 4. Mechanical properties for UD carbon (NCT307-D1-34-600) and woven E-glass (NB307-D1 7781 497A) laminae

Property	**Carbon**	**E-Glass**
E_{11} (GPa)	123	19.2
E_{22} (GPa)	8.2	19.2
E_{33} (GPa)	8.2	11.8
ν_{12}	0.31	0.13
ν_{13}	0.31	0.26
$\nu_{2.3}$	0.31	0.26
G_{12} (GPa)	4.71	3.95
G_{13} (GPa)	4.71	3.43
G_{23} (Gpa)	3.13	3.43
X_T (MPa)	1979	337
X_C (MPa)	1000	497
Y_T (MPa)	59.9	337
Y_C (MPa)	223	497
Z_T (MPa)	59.9	337
Z_C (MPa)	223	497
S (MPa)	103	115
G_{IC} (kJ/mm^2)	0.364	1.829
G_{IIC} (kJ/mm^2)	0.365	2.306

Interfacial strength value of the cohesive elements are determined using the relation proposed by Turon et al. [21]. To determine the interfacial strength of the cohesive layers, length of the cohesive zone must be calculated. With parameters E=8200 MPa, G_c=0.364 kJ/mm^2 and τ^0=59.9 MPa, cohesive zone length is:

$$l_{cz} = 8200\frac{0.364}{59.9^2} = 0.83\ mm$$

To model the cohesive length with 5 elements (N_e^0), the required element length is 0.166 mm, which is highly inefficient in terms of computation time. Instead, interfacial strength is manipulated to model the cohesive length with lower number of elements. Selecting the desired element number as 5 and size as 1 mm:

$$\bar{\tau}^0 = \sqrt{\frac{(8200)\ (0.364)}{1.5}} = 24.4\ MPa$$

$$T = \min\{\tau^0, \bar{\tau}^0\} = 24.4\ MPa$$

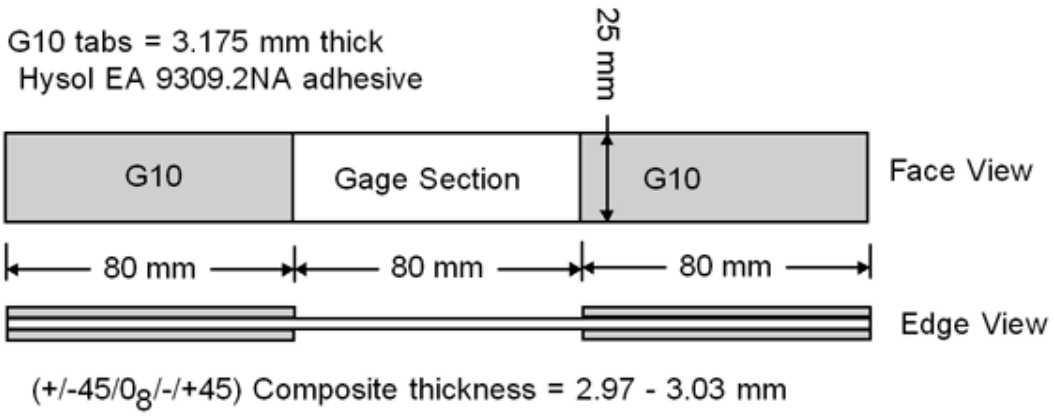

Figure 15. Geometry of the flat specimen [3]

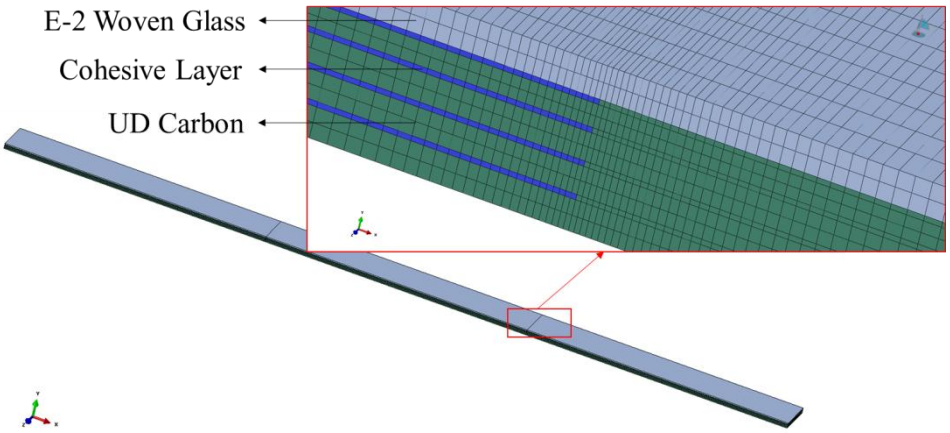

Figure 16. Finite element model of flat specimen

Boundary conditions are applied to simulate the effects of the load-distributing tabs and symmetry. In the stationary tab region, the motion of the nodes on the upper surface of the specimen is held stationary. In the moving tab region, the nodes of the upper surface are constrained such that they can only move in x-direction. Symmetry boundary conditions in Y- and Z- directions are applied to the bottom and side faces of the quarter model, respectively. Boundary conditions applied on the model can be seen in Figure 17.

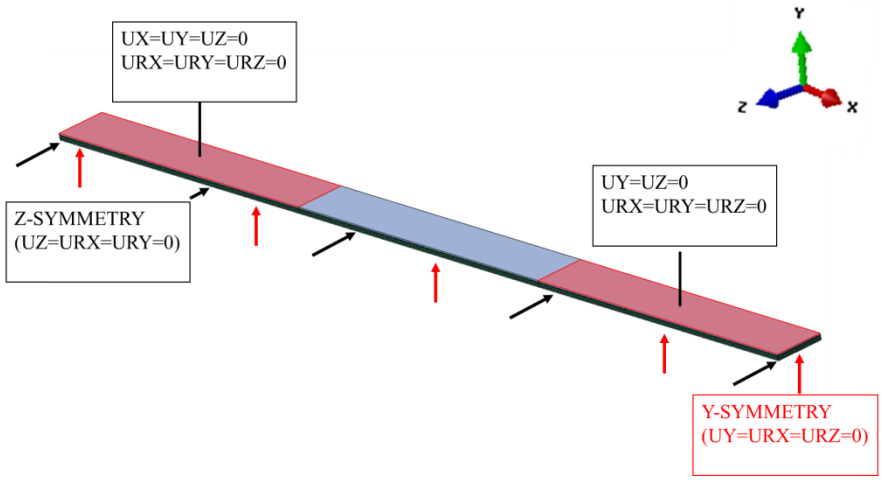

Figure 17. Boundary conditions used for the analysis of flat specimen

Tip displacement is applied to the model using a loading point which is connected to the loading surface via “Kinematic Coupling” option. A tip displacement of 13 mm/s is applied to the loading point until the ultimate failure occurs in the specimen, as it is done in the experimental study. The loading point, loading surface and tip displacement are shown in Figure 18.

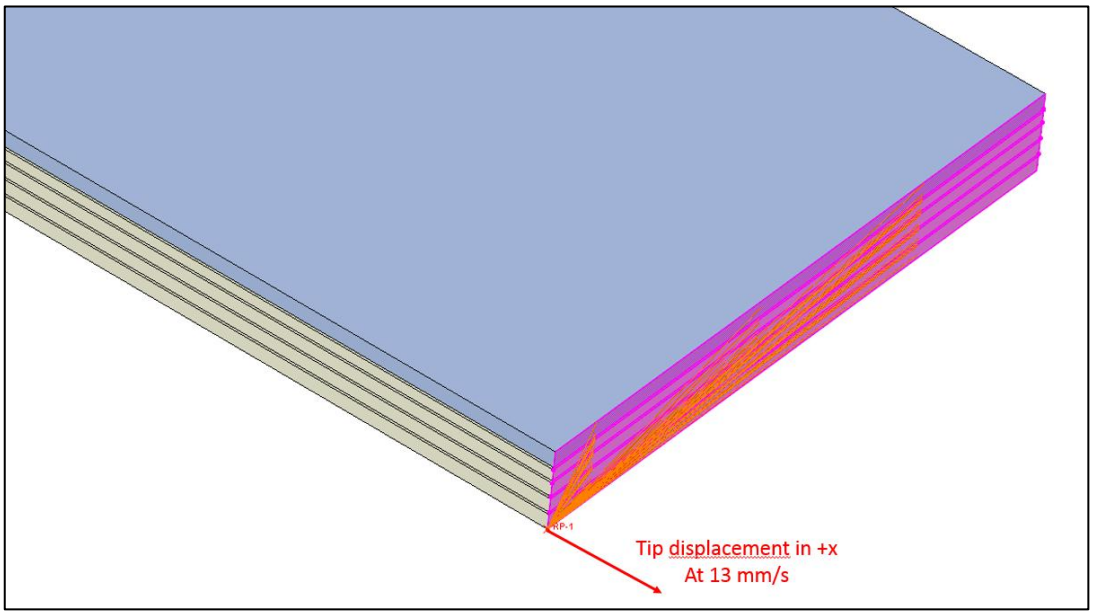

Figure 18. Constraint between loading point-loading surface and the tip displacement applied to the loading point

3.5 Tapered Laminate Model

The tapered laminate has the layup of [±45/02*/09/ 02*/±45] where the superscript ‘*’ indicates the UD carbon plies which are dropped and ±45˚ plies are made of woven E-glass material. A modeling approach similar to the flat model is applied to the tapered specimen. E-Glass and carbon layers are meshed with SC8R continuum shell elements. 0.05 mm-thick cohesive layers are added between the plies in the active

region and meshed with COH3D8 linear hexahedron cohesive elements. The same material configurations are used in the tapered laminate as in the flat specimen, which can be found in Table 4. The details of the tapered laminate can be seen in Figure 20.

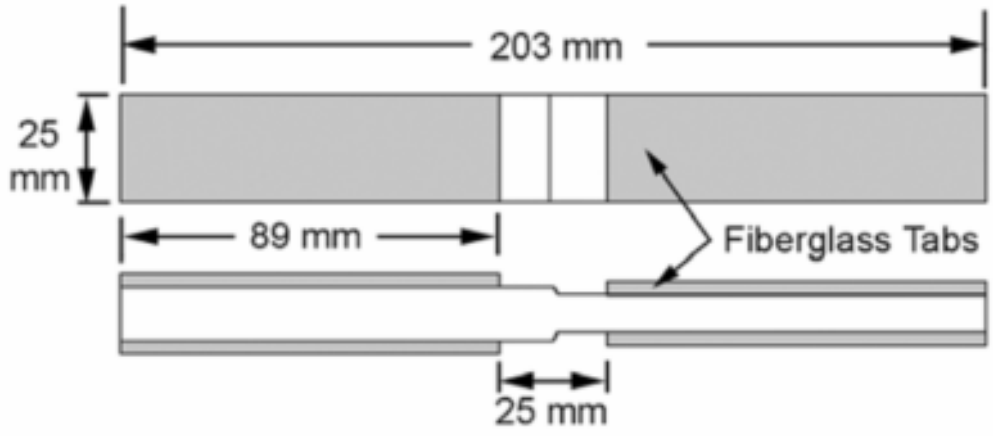

Figure 19. Geometry of the tapered laminate [3]

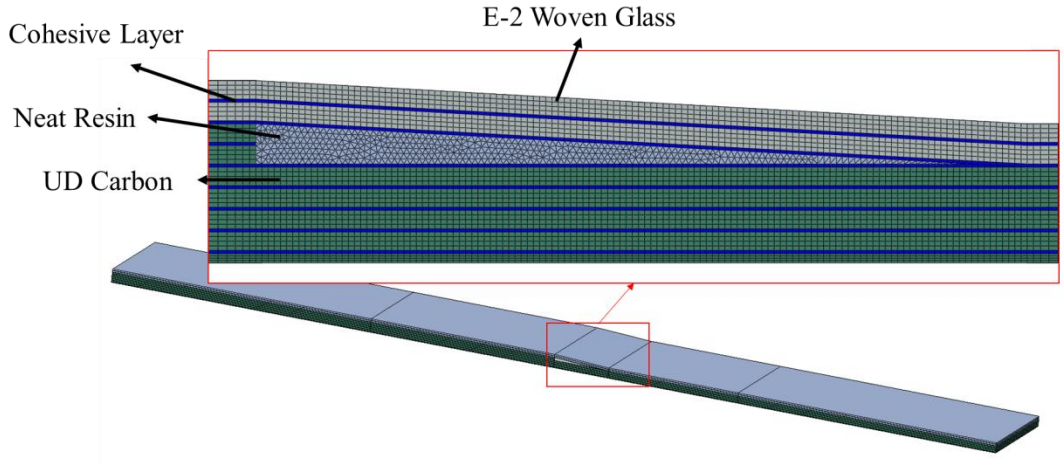

Figure 20. Finite element model of tapered specimen

Boundary conditions are applied to simulate the effects of the load-distributing tabs and symmetry, similar to the application in the flat model. Figure 21 shows the boundary conditions applied to the tapered specimen model.

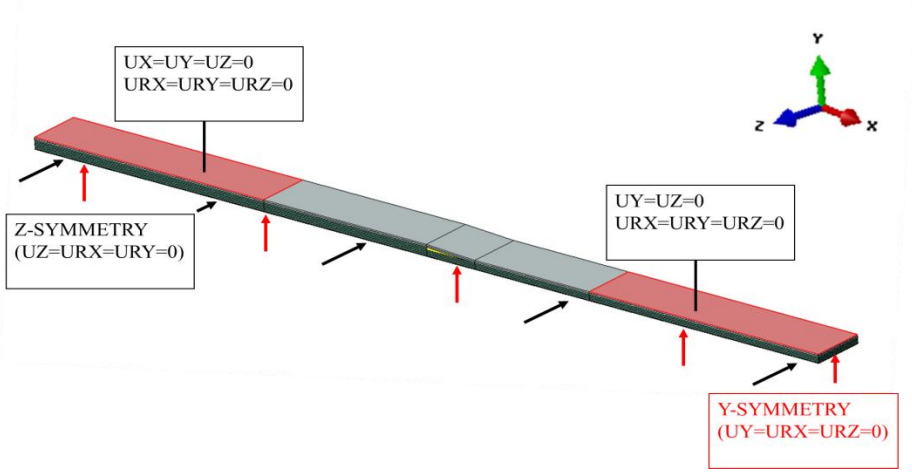

Figure 21. Boundary conditions used for analysis of tapered specimen

3.6 Results

In this study, ultimate strength of a laminate is defined as the point where a sharp decrease in the load carrying capacity is observed (Figure 9). Total reaction force at the loading point is measured to identify this point. Once the ultimate failure moment is captured from the reaction force history, average stresses and strains are measured at that moment from the elements which are close to but not drastically affected from the peak stresses in the failure region.

The failure mode of the flat specimen is tensile fiber failure. Starting from the bottom surface of the glass layers, tensile fiber failure spreads to the carbon layers until the whole section fails. The initiation and evolution of the flat laminate can be seen in Figure 22.

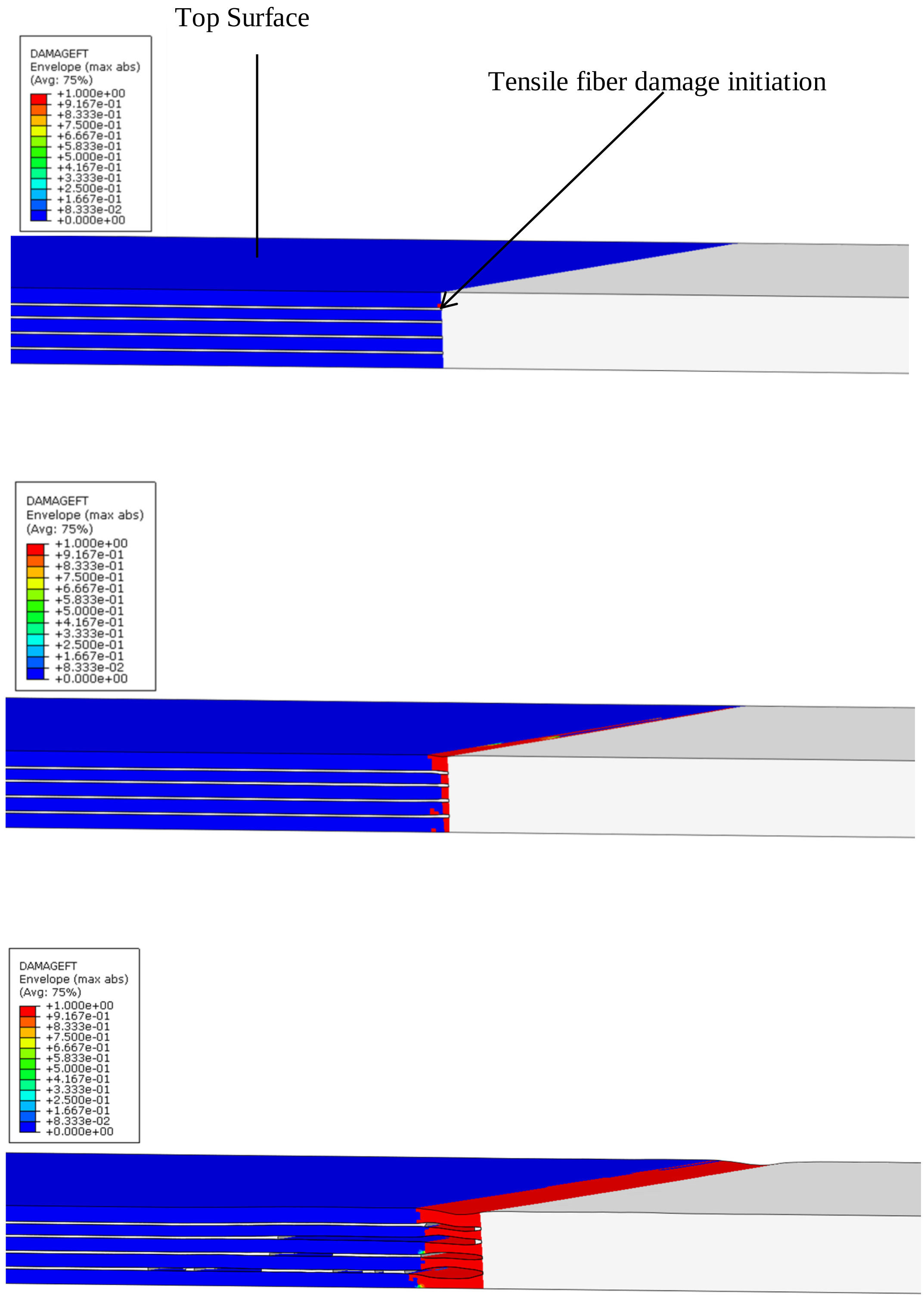

Figure 22. Tensile fiber damage until the ultimate failure of the flat specimen

Failure of the tapered specimen initiates with a delamination crack at the lower corner of the interface between the terminated plies and the resin pocket. The crack evolves between the dropped plies and the core plies. This result is in good agreement with the experimental findings presented in [3]. In Figure 23, crack formation between the dropped 0 degree layers and the 0 degree layers which compose the core section of the tapered laminate can be clearly seen. Figure 24 shows the initiation of damage in the laminate model, with no in-plane damage in the composite layers but a delamination at the location expected from the experimental result. Following the crack at the lower portion of the dropped ply-resin pocket interface, another crack starts at the interface between the resin pocket and the belt plies. Extension of both cracks separates the resin pocket from the core and belt plies. As shown in Figure 25, during the extension of the cracks, tensile matrix and fiber damage occurs in the glass layers due to the changes in the load path caused by the debonded areas between the glass and carbon layers. With the disintegration of the structure, tensile matrix and fiber failure is observed in the glass layers above the resin pocket. It can be seen in Figure 26 that following the failure of the glass layers, fiber damage occurs in the carbon layers due to the loss of integrity and leads to the ultimate failure of the specimen. In these figures, stiffness degradation of the cohesive elements as the delamination crack occurs is presented such that if the stiffness degradation reaches to unity, the element completely loses its capability to carry loads and form a debonded area between adjacent plies. The same approach is used for the in-plane damage. If the fiber or matrix damage reaches the unity, the element can no longer carry any loads.

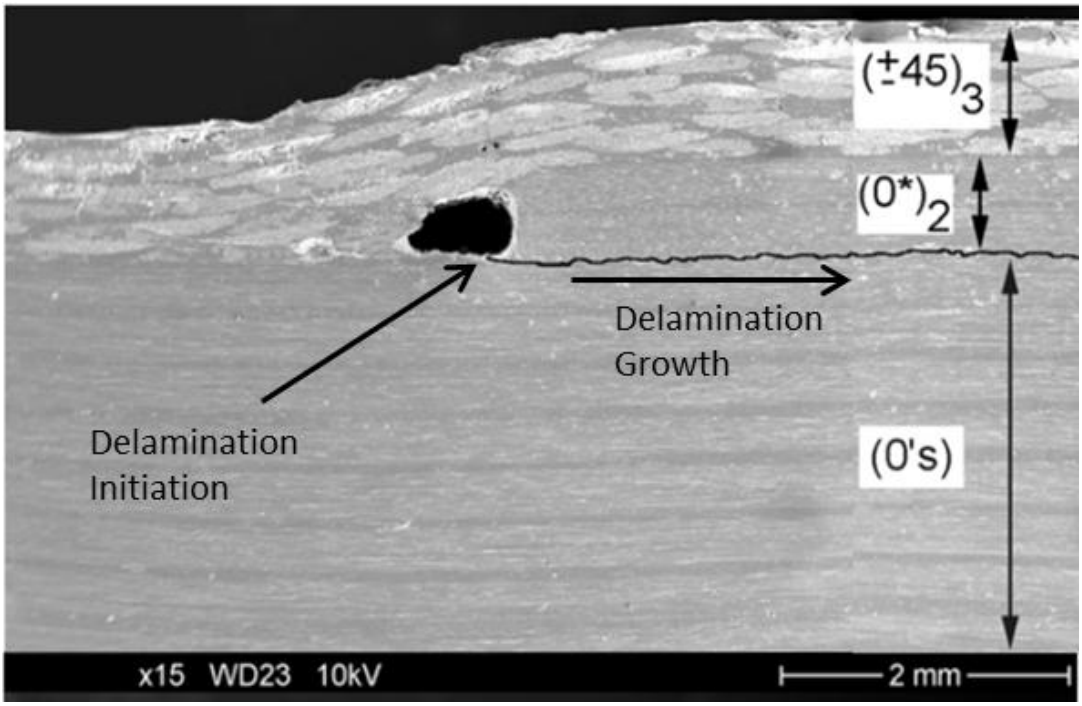

Figure 23. Photograph of the delamination crack of the tapered specimen [3]

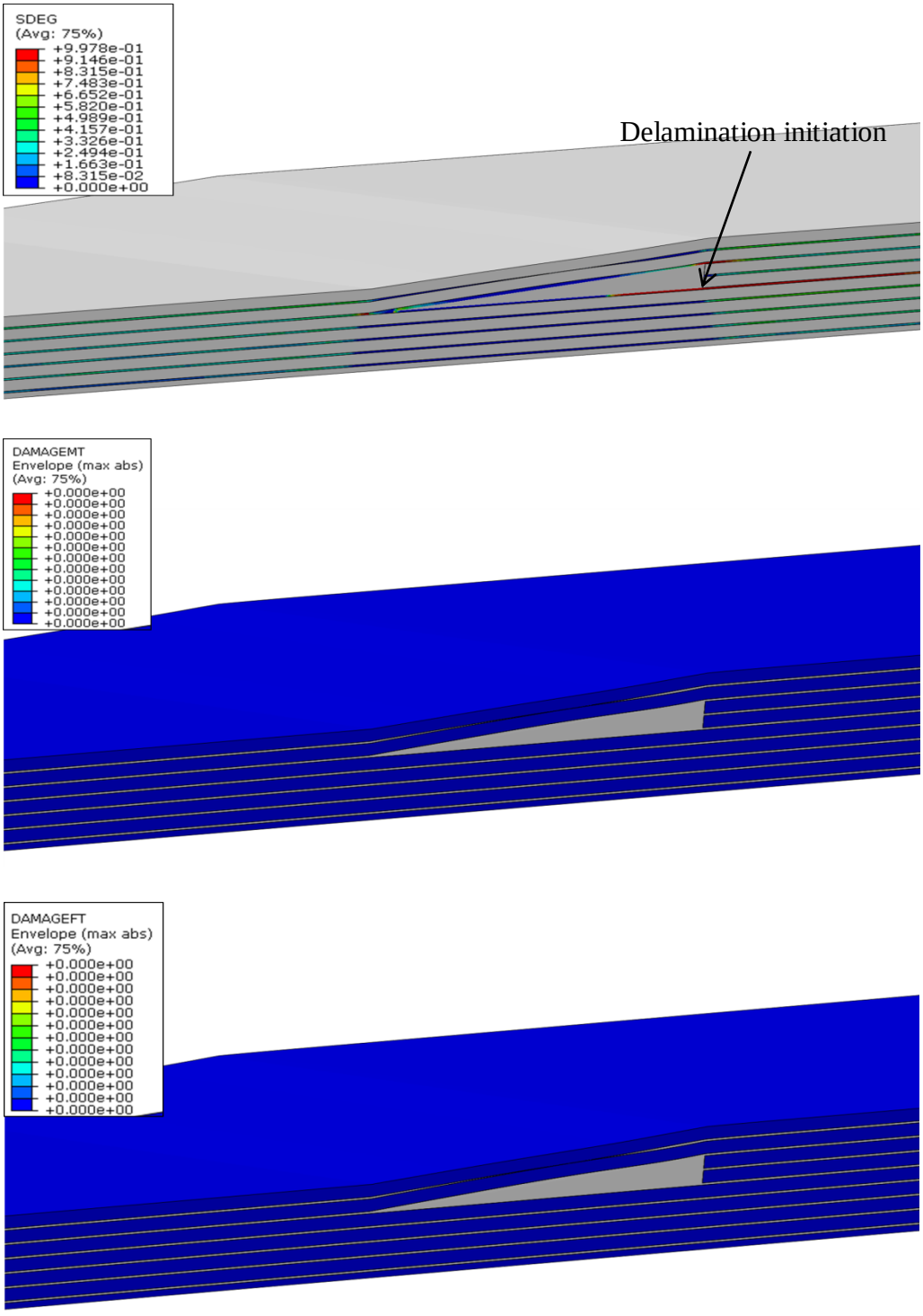

Figure 24. Initiation of damage in the tapered laminate. Top: Stiffness degradation in cohesive layers, Middle: Tensile matrix damage, Bottom: Tensile fiber damage

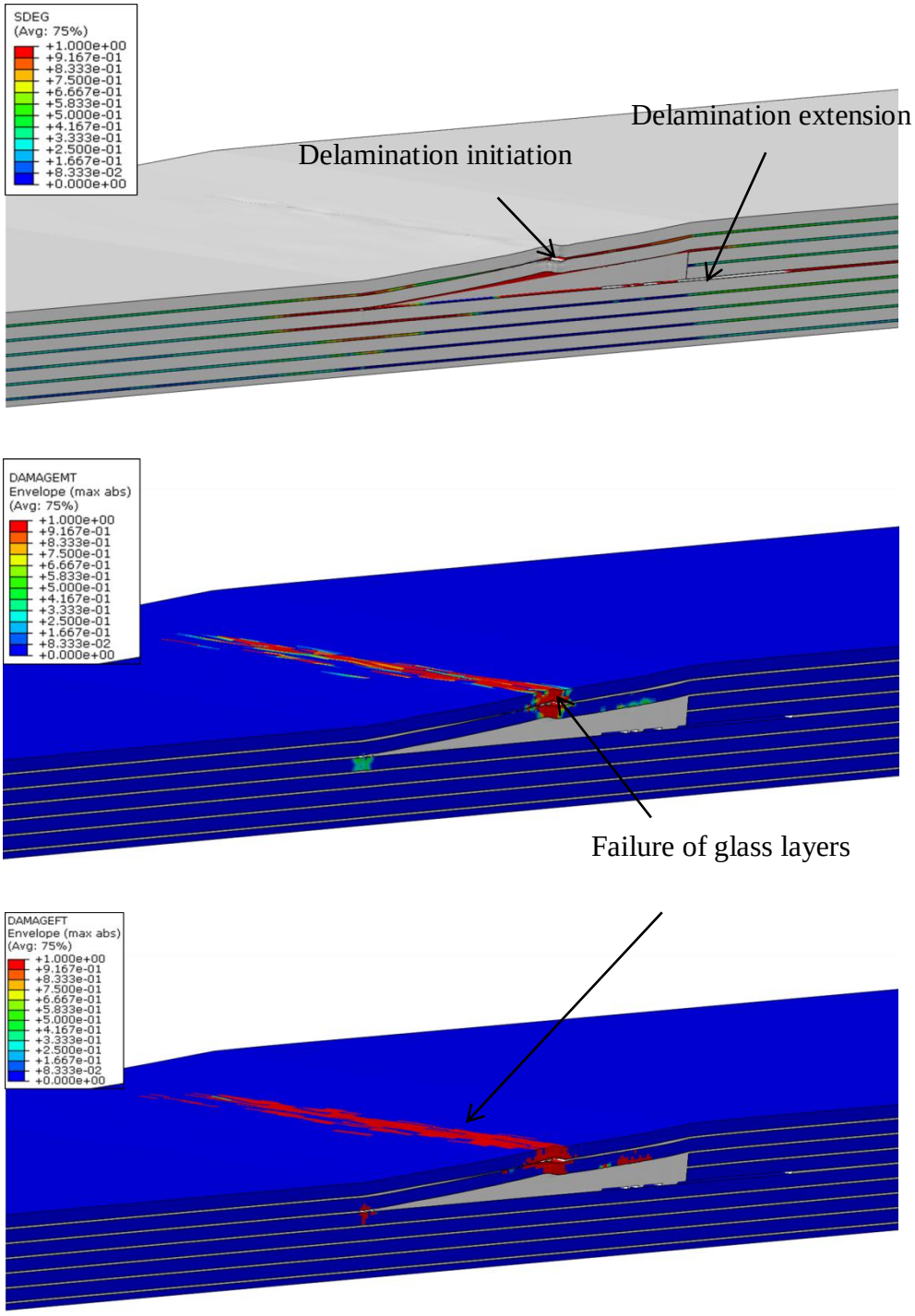

Figure 25. Damage in the tapered laminate as the delamination crack extends in the tapered laminate. Top: Stiffness degradation in cohesive layers, Middle: Tensile matrix damage, Bottom: Tensile fiber damage

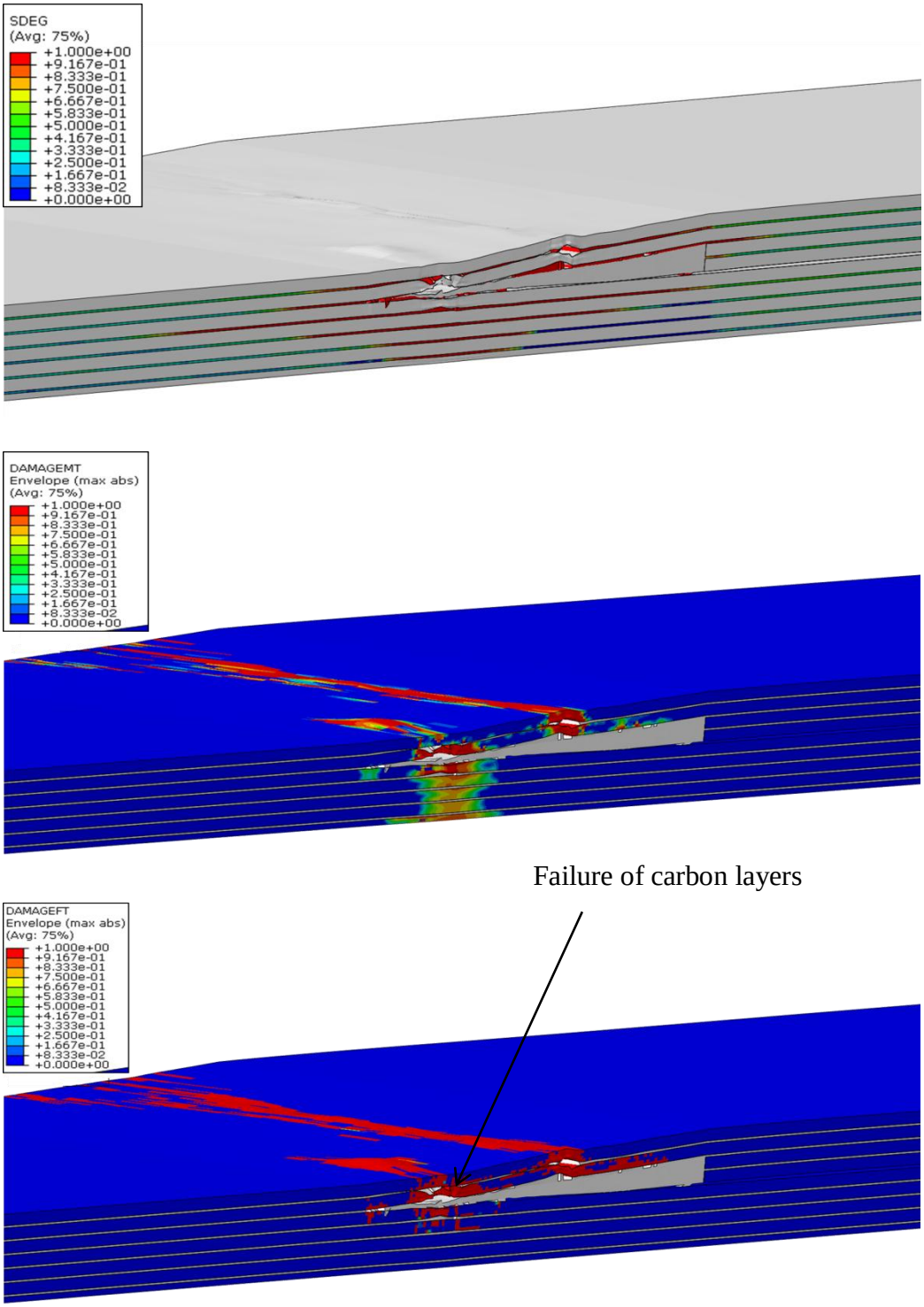

Figure 26. Damage in the tapered laminate at the ultimate failure moment. Top: Stiffness degradation in cohesive layers, Middle: Tensile matrix damage, Bottom: Tensile fiber damage

Stress-strain curves extracted from the PFA and test results are compared in Figure 27 for the flat specimen and Figure 28 for the tapered specimen. For the flat specimen, computational results are observed to have a maximum difference of 4.5% for stresses and 8.5% for strains. For the tapered specimen, results of the progressive failure analysis in terms of stresses are acceptable with a maximum difference of 1.2%. A rather moderate difference of about 16.5% is observed for strains.

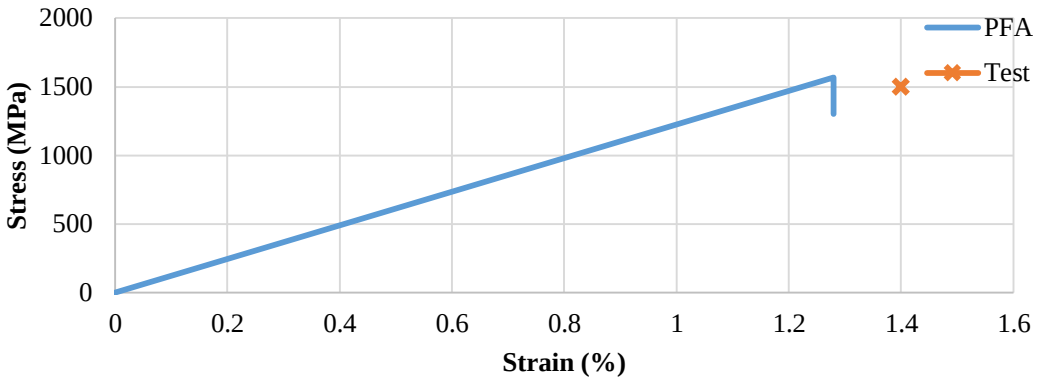

Figure 27. Stress vs strain plots for flat specimen

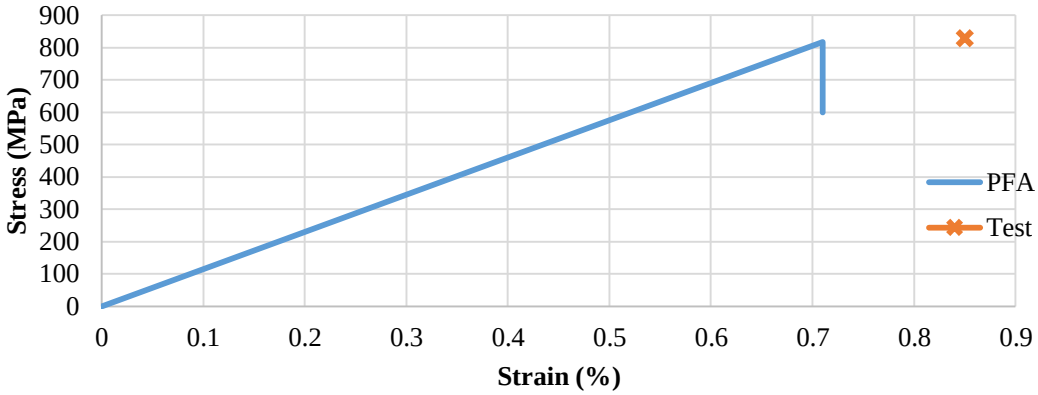

Figure 28. Stress vs strain plots for tapered specimen

The results suggest that the modeling technique proposed in this study is capable of simulating the failure characteristics of a tapered laminate. Both the failure mode and the ultimate tensile strength are successfully predicted. Effects of different design parameters can be observed by modeling with this approach. Building on this modeling technique, different design variables are applied on a sample laminate and the effects on the ultimate load is evaluated in the next chapters.

CHAPTER 4

EXAMINATION OF THE DESIGN CHOICES FOR A SELECTED LAMINATE

The designer must make a number of choices in the preliminary design phase of a composite structure including a tapered section. Drop off configuration, drop length, core/belt ply counts and dropped ply count at a station are the main design parameters. These parameters are visualized on a laminate scheme in Figure 29. Many different design solutions can be reached within the boundaries of the tapered region. To have an efficient design, it is crucial to determine the effects of several design parameters on the ultimate strength of the laminate. In this section, different design choices are examined by determining the ultimate tensile load values by the failure analysis method described in Chapters 3.2 and 3.3.

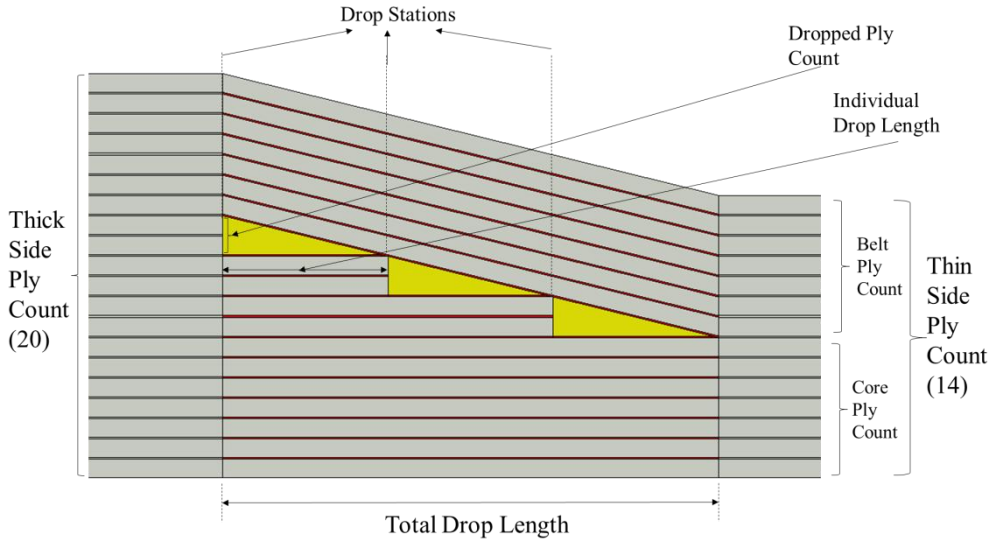

Figure 29. Parameters of a laminate (numbers in parentheses show the value of the parameters with constant values) (Shown in half-view)

Python scripts are used to create finite element models, run the analyses and post-process the results automatically. Over 250 analyses are performed to generate data to characterize the effects of the design choices. A sample python script is given in Appendix.

A laminate with 40 plies (9.8 mm) at the thick end and 28 plies (6.9 mm) at the thin end, whose schematic is shown in Figure 29, is chosen for the study. The laminate is fixed at the thick end and pulled at the thin end as shown in Material of the laminate is selected as carbon, whose material properties are given in Table 4. Laminates at this thickness are commonly used in composite structures in rotorcraft. The geometry of the laminate is idealized such that no voids, wrinkles or curvatures are present since the aim is to investigate the effects of preliminary design variables. Models with different design variables are compared to observe how the ultimate load is affected. The study involves two drop-off configurations which are mentioned by Fish and Vizzini [8], namely the staircased-grouped (SG) and the staircased-dispersed (SD). Schematic drawings of these configurations can be seen in Figure 31. These two configurations are selected since they represent two main choices in the design procedure. In the SG configuration, the dropped plies can be located closer to the mid-plane of the laminate. However, resin pockets are connected to each other in this configuration. Contrarily, in the SD configuration, the resin pockets are separated from each other but the dropped plies cannot be placed near the mid-plane as it can be done in the SG configuration. Drop length is the parameter that is changed in both of the configurations. The study also includes two other parameters which are changed only in the staircased-grouped configuration: the belt/core ply counts and how many plies are dropped off at a drop section.

Figure 30. Schematic of the fixed and loaded ends of the tapered laminates

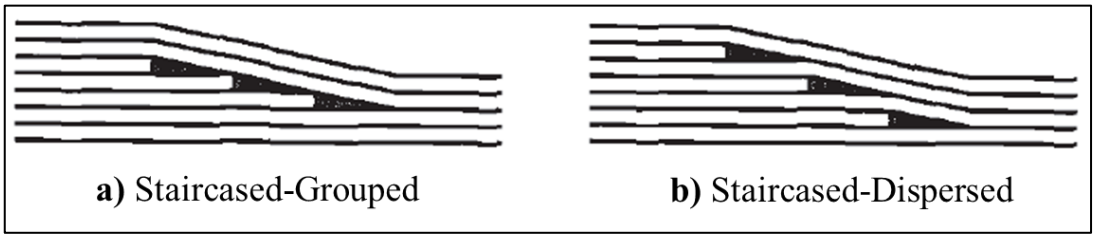

Figure 31. Different ply configurations used in the parametric study [8]

Similar to the benchmark study, the ultimate load for a laminate is determined by examining the history of the reaction force on the loading point. The point after which a sharp decrease in the reaction force is captured is accepted as the ultimate load point. Then, the results are presented in a non-dimensional form by dividing the ultimate load of a 28-ply flat laminate with the same material properties, which is obtained through the same analysis procedure.

The laminate is composed of unidirectional carbon layers. Mechanical properties of the carbon layers are given in Table 4. Properties of the cohesive elements are calculated by using equations (2-1), (2-3) and (2-4). In-plane and out-of-plane damage models are implemented as described in sections 3.2 and 3.3. Progressive failure algorithm described in Figure 10 is used to degrade intralaminar and interlaminar material properties up to the ultimate failure.

4.1 Drop-Off Configuration

Two different drop-off configurations represent the cases in which the dropped plies are grouped or separated from each other. The comparison is made for the same drop lengths and dropped ply counts at a drop station which is equal to 1. Figure 32 shows finite element models of the two configurations with same thick/thin ply counts and total drop lengths.

Since there are 13 combinations for constant drop length and constant dropped ply count at a drop station (from 1 belt/13 core plies to 13 belt/1 core plies), ultimate load values of the SD laminates are compared with the average of the 13 SG configurations at each total drop length.

4.2 Total Drop Length

The parametric study on the drop length is done for both configurations separately. Total drop length of 30, 60 and 90 mm are used for comparison. Geometries created by the change in the drop length for SD and SG configurations are shown schematically in Figure 33. Average values of 13 combinations with respect to belt/core ply counts are used for each dropped ply count for the SG combination.

4.3 Belt/Core Ply Count

Belt and core plies are continuous plies which are closer to the inner and outer surface of the laminate, respectively (Figure 29). In this part of the parametric study, the effect of the count of the belt and core plies for the same number of dropped plies is

investigated for the staircased-grouped configuration. Figure 34 shows how the count of these plies can be adjusted by changing the location of the dropped ply group.

4.4 Dropped Ply Count at a Drop Station

The plies can be terminated either individually or in the forms of groups. This can be done either keeping a constant total drop length by increasing the individual drop length as dropped ply count increases or decreasing the total drop length by keeping the individual drop length constant while increasing the dropped ply count. Both cases are investigated in this section of the parametric study. In Figure 35, how the geometry of the laminate is affected by the changes mentioned above can be seen.

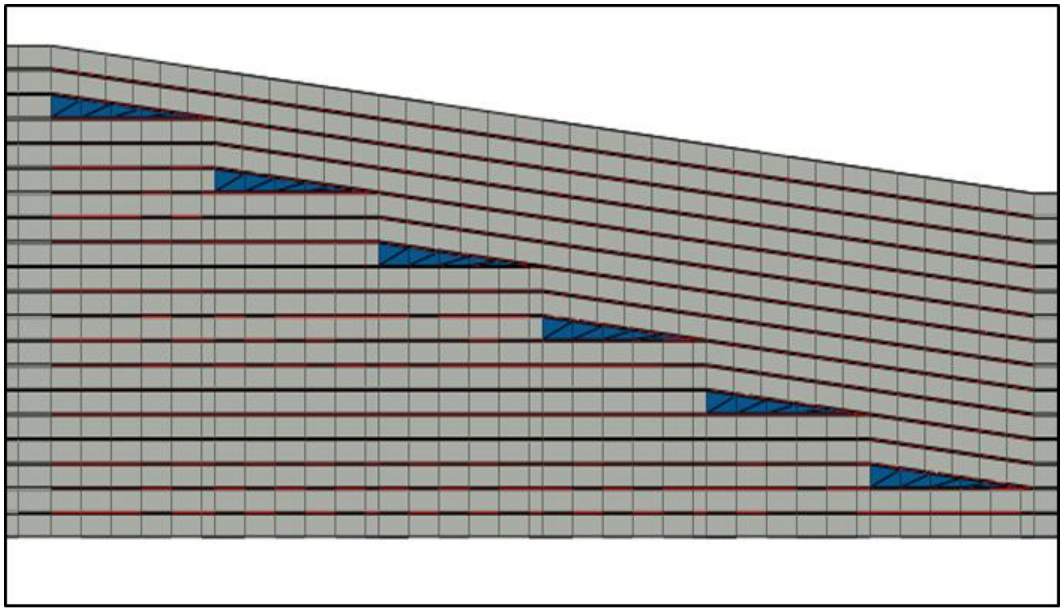

a)

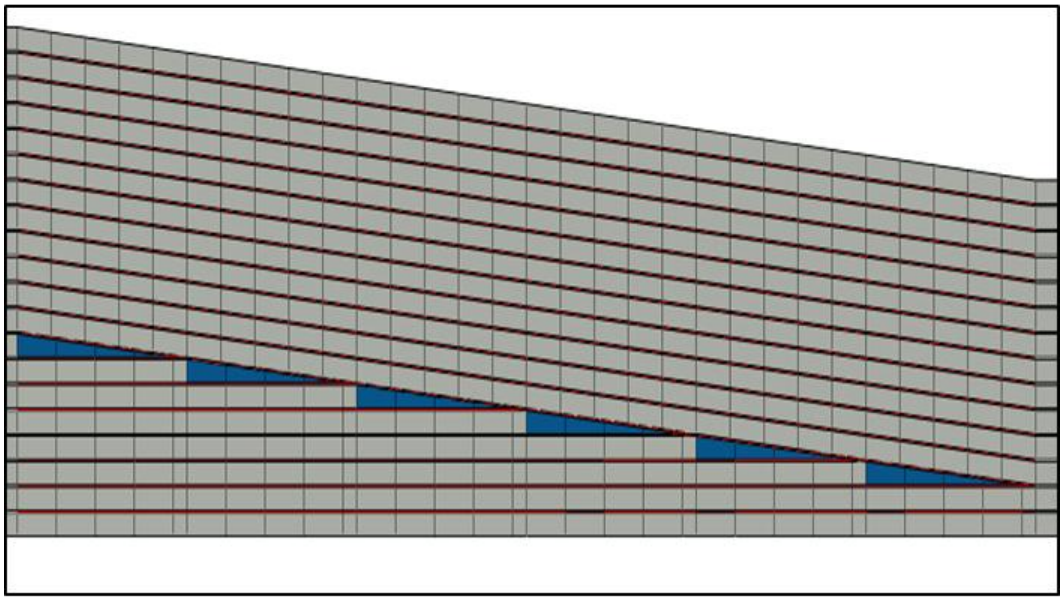

b)

Figure 32. Finite element mesh of the two different drop-off configurations: a) Staircased-dispersed, b) Staircased-grouped

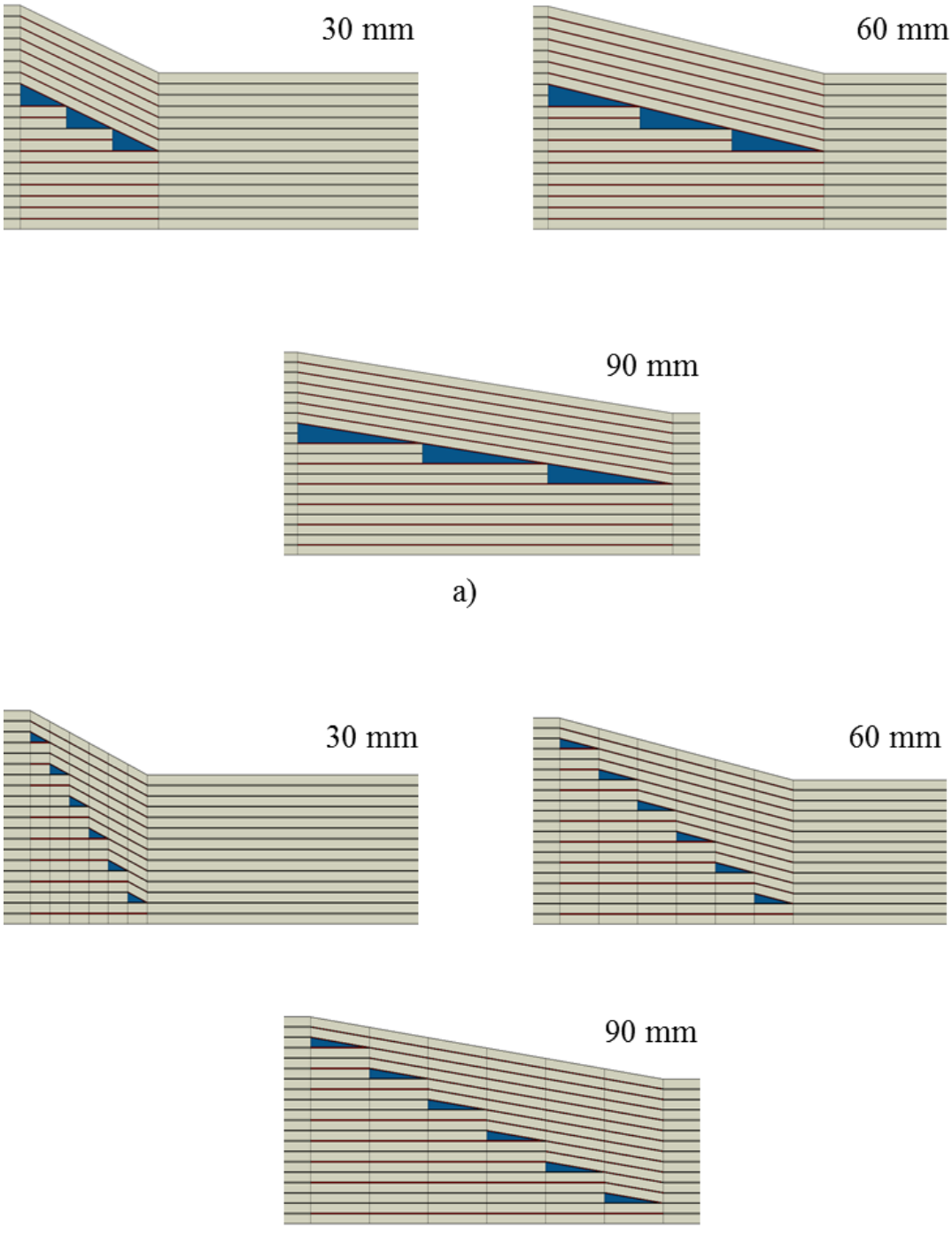

Figure 33. Increase in drop length for a) SG b) SD configurations

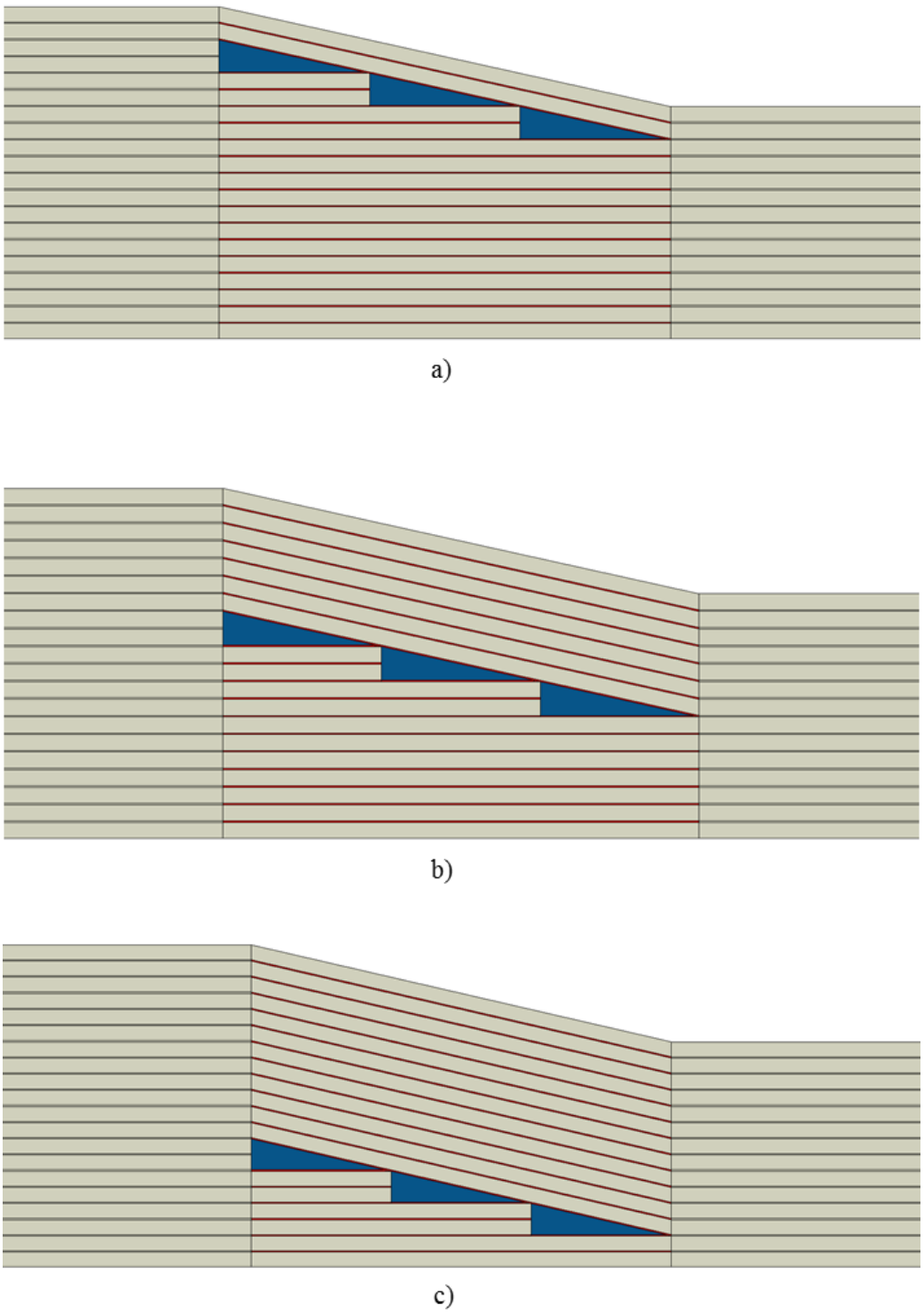

Figure 34. Different belt/core ply counts for constant thick and thin end ply counts: a) 2 belt/12 core, b) 7 belt/7 core, c) 12 belt/2 core plies

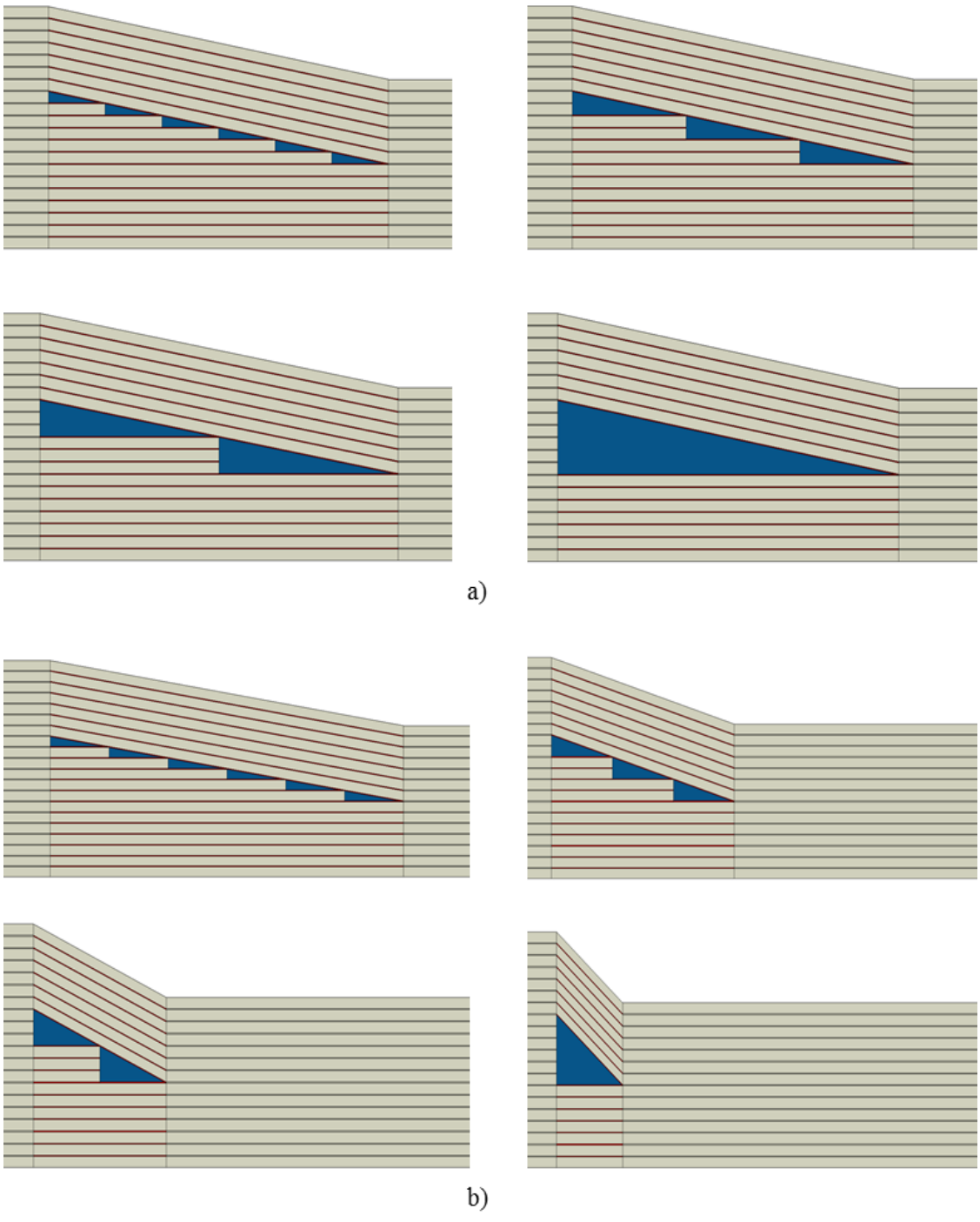

Figure 35. Laminates with different dropped ply counts at a station: a) Fixed total drop length, b) Fixed individual drop length

CHAPTER 5

RESULTS

In this chapter, the results of the parametric study described in Chapter 4 are presented. Effects of the drop-off configuration, total drop length, belt/core ply count and dropped ply count at a drop station on the ultimate tensile strength of the laminate are evaluated based on the results.

5.1 Drop-Off Configuration

The SD and SG configurations differ in the delamination paths up to the ultimate failure. In the SD configuration, due to the effect of the connected resin pockets, delamination cracks grow on the interface of all of the resin pockets with the belt plies and on the top surface of the core plies. On the other hand, cracks grow around each dropped ply and the following resin pocket in the laminates with the SG configuration. These results are in good agreement with the findings of Fish and Vizzini [8]. Figure 36 shows the delamination paths observed in [8] and predicted by the progressive failure algorithm used in this study.

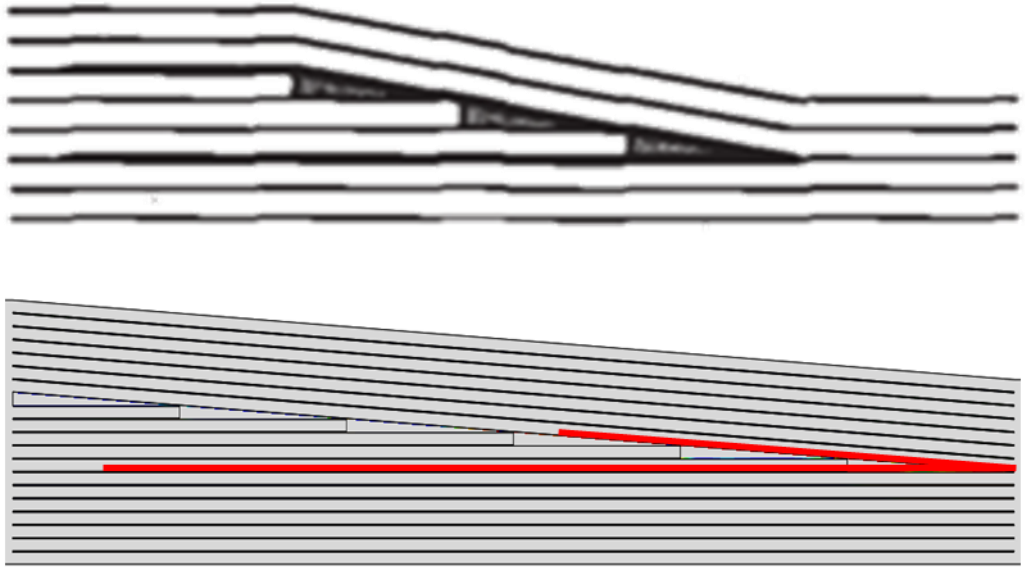

a)

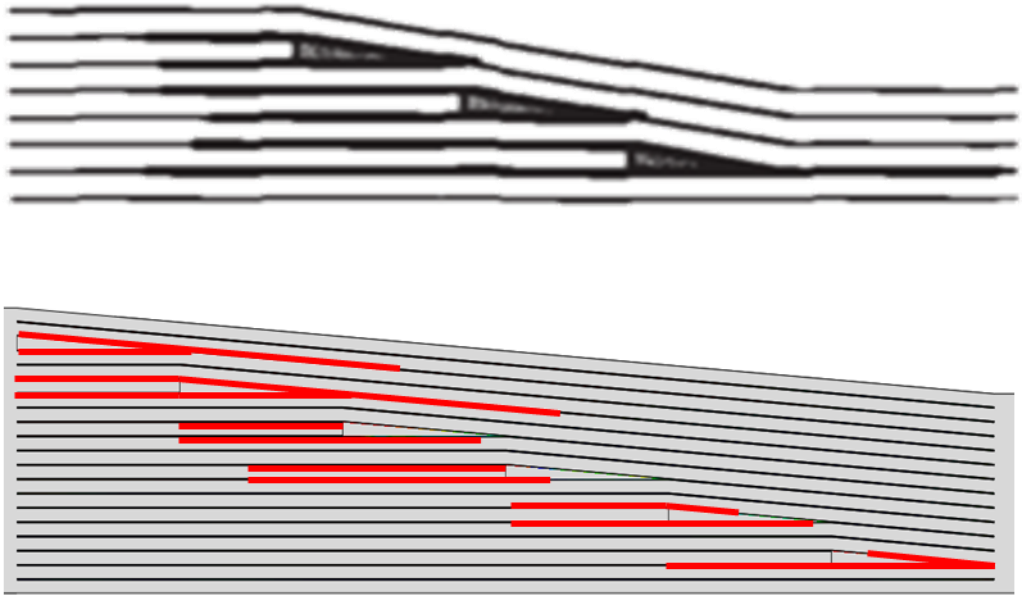

b)

Figure 36. Comparison of the delamination paths from [8] (top) and the PFA (bottom)

Ultimate tensile loads for two different configurations at each total drop length are presented in Table 5 and Figure 37. The results indicate that the selection of the drop-off configuration changes the ultimate tensile load of the laminate up to 1.6 % within the total drop length range of the parametric study. At every total drop length, the SD configuration has a slightly higher ultimate tensile load than that of the equivalent SG configuration. This can be explained by the connected neat resin regions in the SG configuration, which can decrease the integrity of the laminate as a whole and ease crack propagation.

Table 5. Variation of the non-dimensional ultimate tensile load (%) for SD and SG configurations at different total drop lengths

Drop Configuration \ Total Drop Length	30 mm	60 mm	90 mm
SD	103.2	109.2	111.6
SG (Average)	102.8	108.4	109.9

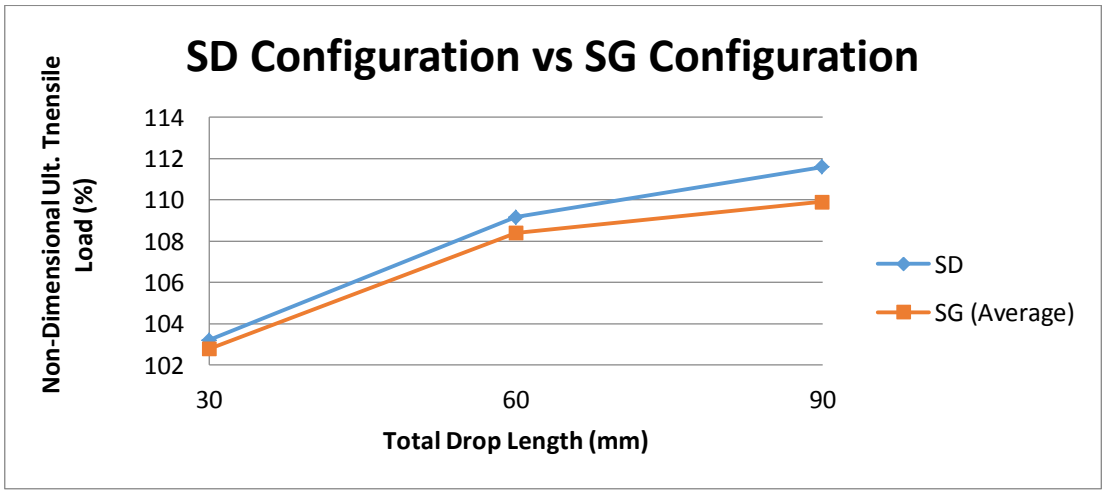

Figure 37. Effects of the drop configuration on tensile strength

5.2 Total Drop Length

Ultimate tensile loads for two different configurations at each total drop length are presented in Table 6 and Figure 38. A clear increase in the ultimate load is observed with increasing total drop length. In the range of this parametric study, up to 8.4% increase is observed. This is due to the fact that the axial stiffness variation gets smoother as the drop length increases. Effects of the stress singularities caused by the drop-offs are more influential for short drop lengths.

Table 6. Variation of the non-dimensional ultimate tensile load (%) with varying total drop length

Total Drop Length (mm) / Drop Configuration	30	60	90
SD	103.2	109.2	111.6
SG-1 drop at a drop station	102.8	108.4	109.9
SG-2 drops at a drop station	101.6	107.6	110.1
SG-3 drops at a drop station	102.3	107.6	110.6
SG-6 drops at a drop station	101.8	107.4	110.6

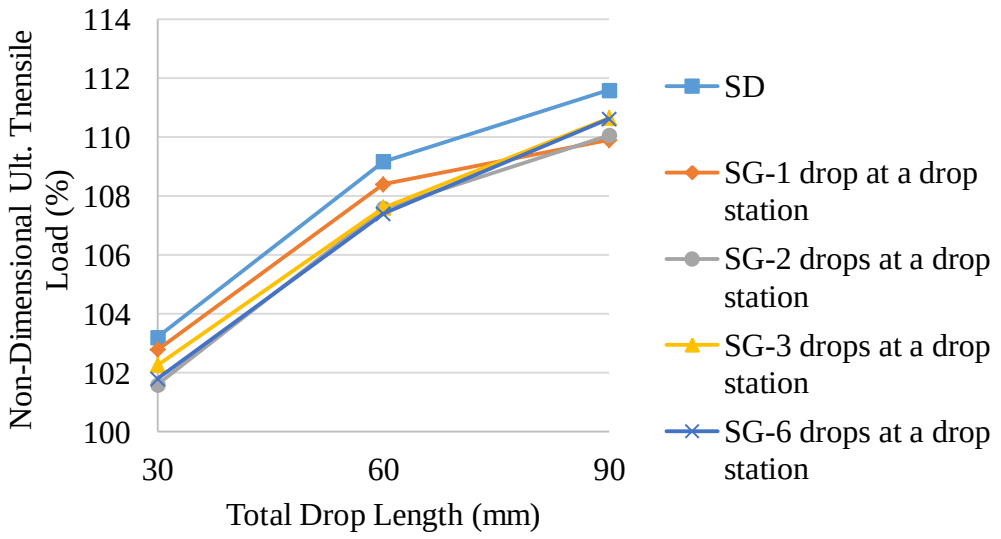

Figure 38. Effects of the total drop length on tensile strength

5.3 Belt/Core Ply Count

The results are presented for varying dropped ply count at a station for constant total drop length. Different characteristics are observed for different total drop lengths. For the total drop length of 30 mm, ultimate tensile load tends to increase for all types of laminates as the belt ply count increases. Figure 39 shows the general trend of increase as the dropped plies are moved closer to the mid-plane for laminates with 30 mm of total drop length. For shorter configurations, location of the dropped ply group can affect the ultimate tensile load up to 4.8%. Figure 40 shows the ultimate load values for 60 mm total drop length. For rather moderate total drop length values, the effect of belt/core ply counts diminishes as the ultimate tensile load results scatter around an almost fixed mean value. For 90 mm drop length, it is difficult to reach a conclusion on the position of the dropped plies, as the scatter is very high and no clear trend is observed. The variation of the ultimate tensile load for 90 mm total drop length can be seen in Figure 41.

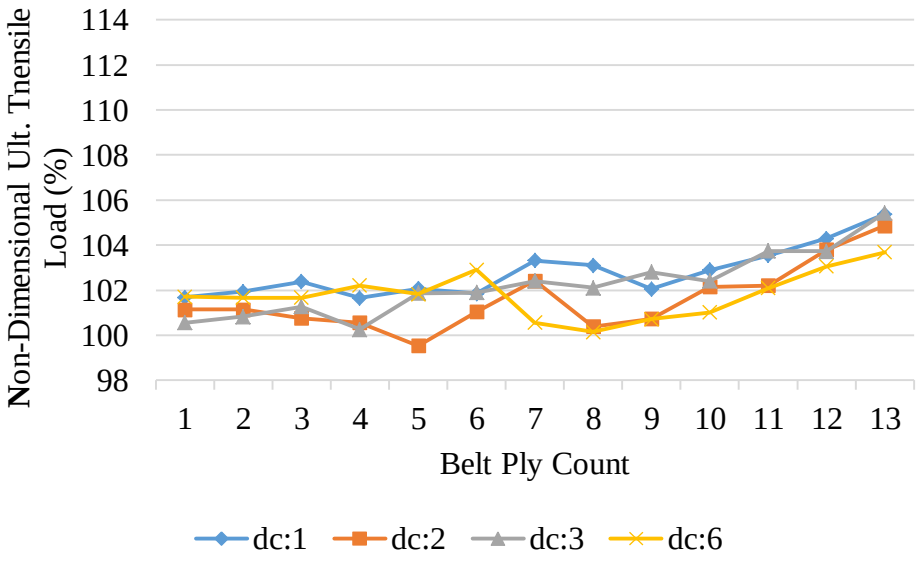

Figure 39. Effects of the belt ply count for the total length of 30mm (dc: dropped ply count at a drop station)

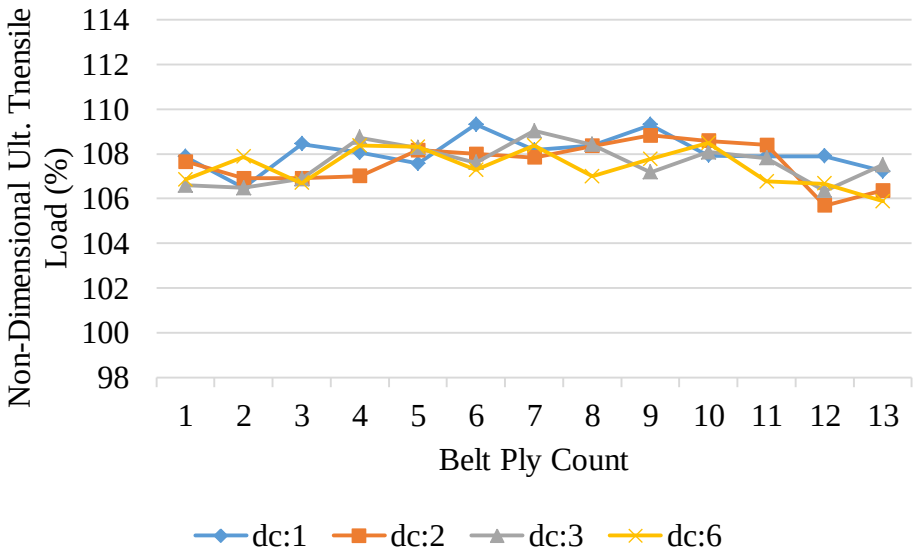

Figure 40. Effects of the belt ply count for the total length of 60 mm (dc: dropped ply count at a drop station)

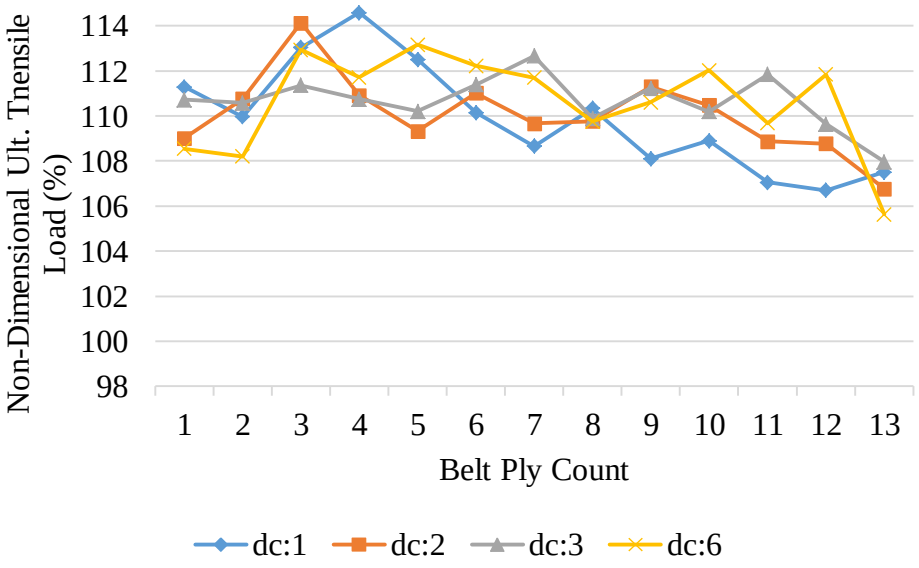

Figure 41. Effects of the belt ply count for the total length of 90 mm (dc: dropped ply count at a drop station)

5.4 Dropped Ply Count at a Drop Station

The results of this part of the parametric study show that with constant total drop length, dropped ply count at a drop station has low effect on the ultimate tensile load. From Table 7, it can be seen that the maximum difference between the ultimate tensile loads among the constant total drop lengths of 30, 60 and 90 mm is 1.2%. Figure 42 also shows the almost horizontal trend for the ultimate tensile load as the dropped ply count changes. However, the picture changes if the constant parameter is set to the individual drop length rather than the total drop length. If this is the case, the ultimate tensile load is affected drastically with increasing dropped ply count at a station.

Table *8* shows that the ultimate tensile load can decrease as much as 16.6% and Figure 43 shows a clear decreasing regime as the dropped ply count at a station increases. The reason for that definite decrease in strength can be explained by the combined effect of the stress singularity caused by the termination of multiple plies and the decreased total drop length.

Table 7. Variation of the non-dimensional ultimate tensile load (%) with varying drop count at a drop station for constant total drop length

Drop Configuration \ Total Drop Length (mm)	30	60	90
SG-1 drop at a drop station	102.8	108.4	109.9
SG-2 drops at a drop station	101.6	107.6	110.1
SG-3 drops at a drop station	102.3	107.6	110.6
SG-6 drops at a drop station	101.8	107.4	110.6

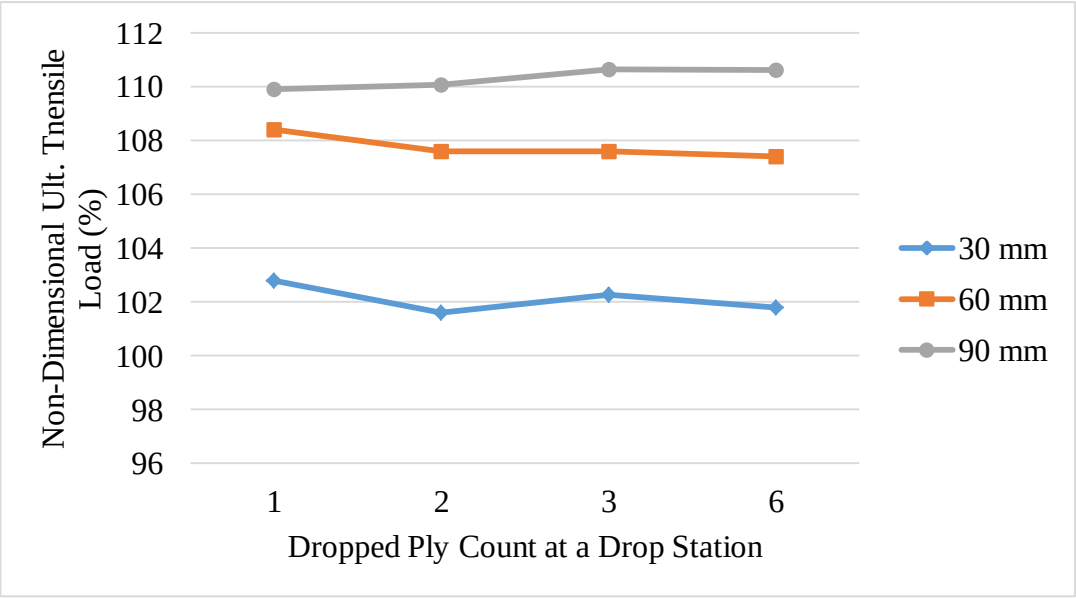

Figure 42. Effects of the dropped ply count at a station for constant total drop length

Table 8. Variation of the non-dimensional ultimate tensile load (%) with varying drop count at a drop station for constant individual drop length

Drop Configuration \ Individual Drop Length (mm)	5	10	15
SG-1 drop at a drop station	102.8	108.4	109.9
SG-2 drops at a drop station	95.6	101.6	105.3
SG-3 drops at a drop station	91.3	98.6	102.3
SG-6 drops at a drop station	88.2	94.5	96.9

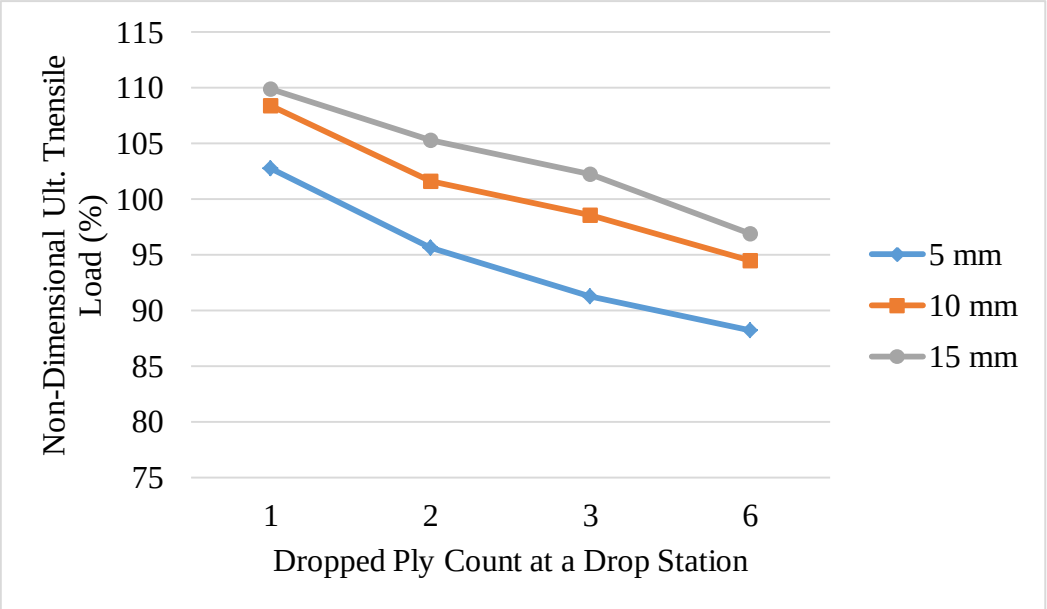

Figure 43. Effects of the dropped ply count at a station for constant individual drop length

CHAPTER 6

CONCLUSION AND FUTURE WORK

Tensile strength of tapered laminates is affected by a number of parameters. These parameters create a pool of different design selections for a given thick and thin side ply counts. In this study, effects of these parameters are investigated with a progressive failure algorithm involving in- and out-of-plane failure mechanisms. In-plane failure modes of the composite layers are modeled with Hashin failure criteria and delamination phenomenon is modeled with cohesive layer elements. The numerical method is validated through comparison with experimental results from literature. The failure mode and the ultimate strength values obtained from the numerical simulation procedure were similar to that of the test results. Many progressive failure analyses have been done via scripts written in Python programming language to automatically create the finite element models of the laminates and post-process the results. The outputs of the parametric study offer the following conclusions:

- The choice of drop configuration slightly affects the ultimate tensile strength of the laminate. Choosing dispersed configuration instead of grouped configuration increases the ultimate strength by 1.6%.
- Total drop length is the most dominant parameter, which can create a difference of 8.4% in the range of the parametric study. This is due to the smooth stiffness change at the drop location as the drop length increases.
- For configurations with short drop lengths, increasing the belt ply count; in other words, moving the dropped plies to the mid-plane increases the ultimate strength by 4.8%. As the drop length increases, no clear trends can be observed for increasing belt ply count.

- The number of plies dropped at a station does not significantly affect the ultimate strength if the total drop length is kept constant. However, if the individual drop length is fixed, a severe decrease in the ultimate strength is observed, ranging up to 16.6%. This is a result of both the increased stress concentration as the dropped ply count is increased and the sharp stiffness change along the tapered region as the total drop length is decreased.

To conclude, it is beneficial to choose the staircased-dispersed configuration and increase the total drop length for the ultimate tensile strength of the laminate. For the cases where the total drop length is rather short (≈50-150 times the drop thickness), the more the dropped plies are close to the mid-plane, the higher the ultimate tensile strength of the laminate. Finally, total drop length of the laminate should be kept at least constant if a group of plies are dropped at a drop station since the ultimate strength is severely decreased if the total drop length decreases in such a situation.

With this study, different failure mechanisms of a tapered composite laminate

has been successfully implemented to a finite element methodology. The methodology provides an improvement to the efforts to predict the behavior of tapered laminates up to ultimate failure.

The future work that can be established on the results of this study are summarized as follows:

- The trend curves obtained from the parametric study must be validated with a test campaign. Ultimate tensile strengths of tapered laminates produced with different design variables should be determined with tensile tests and the results have to be compared with numerical results.

- An optimization code can be developed to find the strongest drop-off design for given fixed parameters. Such a code would ease the preliminary design of tapered composite structures.
- Effects of non-linear stiffness degradation procedures for in-and-out-of-plane damage mechanisms can be studied.

REFERENCES

[1] G. B. Murri, J. R. Schaff, and A. L. Dobyns, "Fatigue and Damage Tolerance Analysis of a Hybrid Composite Tapered Flexbeam," in *American Helicopter Society Forum*, 2001.

[2] Z. Hashin, "Failure Criteria for Unidirectional Fiber Composites," *J. Appl. Mech.*, vol. 47, no. 2, p. 329, 1980.

[3] D. D. Samborsky, T. J. Wilson, P. Agastra, and J. F. Mandell, "Delamination at Thick Ply Drops in Carbon and Glass Fiber Laminates Under Fatigue Loading," *J. Sol. Energy Eng.*, vol. 130, no. 3, p. 22, 2008.

[4] S. V Hoa, J. Daoust, and B. L. Du, "lnterlaminar Stresses in Tapered Laminates," in *Polymer Composites*, 1988, pp. 337–344.

[5] E. A. Armanios and L. Parnas, "Delamination analysis of tapered laminated composites under tensile loading," in *Composite materials: Fatigue and Fracture Volume 3*, vol. 3, 1991, pp. 3440–358.

[6] S. A. Salpekar, I. S. Raju, and T. K. O'Brien, "Strain-Energy-Release rate Analysis of the End-Notched Flexure Specimen Using the finite Element Method," *Nasa Tech. Memo.*, no. November 1987.

[7] J. M. Curry and E. R. Johnson, "Effect of Dropped Plies on the Strength of Graphite-Epoxy Laminates," *AIAA J.*, vol. 30, no. 2, pp. 449–456, 1992.

[8] J. C. Fish and A. J. Vizzini, "Delamination of Ply-Drop Configurations," *Compos. Mater. Test. Des. (Eleventh Vol.*, pp. 323–332, 1993.

[9] M. R. Wisnom, M. I. Jones, and W. Cui, "Failure of tapered composites under static and fatigue tension loading," *AIAA J.*, vol. 33, no. 5, pp. 911–918, 1995.

[10] A. J. Vizzini and S. W. Lee, "Damage Analysis of Composite Tapered Beams," *J. Am. Helicopter Soc.*, vol. 40, no. 2, p. 43, 1995.

[11] D. Carrella-Payan, L. F. Kawashita, and G. Allegri, “Tensile Testing Characterization of Asymmetrically Tapered Composite Laminates,” in *18th International Conference on Composite Materials*, 2011.

[12] Z. Petrossian and M. R. Wisnom, “Parametric study of delamination in composites with discontinuous plies using an analytical solution based on fracture mechanics,” *Compos. Part A Appl. Sci. Manuf.*, vol. 29, no. 4, pp. 403–414, 1998.

[13] G. I. Barenblatt, “The Mathematical Theory of Equilibrium Cracks in Brittle Fracture,” *Adv. Appl. Mech.*, vol. 7, no. C, pp. 55–129, 1962.

[14] D. S. Dugdale, “Yielding of steel,” *J. Mech. Phys. Solids*, vol. 8, pp. 100–104, 1960.

[15] A. Hillerborg, M. Modeer, and P.-E. Petersson, “Analysis of crack formation and crack growth in concrete by means of fracture mechanics and finite elements,” *Cement and Concrete Research*. pp. 773–782, 1976.

[16] A. Turon, P. P. Camanho, J. Costa, and C. G. Davila, “A damage model for the simulation of delamination in advanced composites under variable-mode loading,” *Mech. Mater.*, vol. 38, no. 11, pp. 1072–1089, 2006.

[17] P. P. Camanho, C. G. Davila, and D. R. Ambur, “Numerical Simulation of Delamination Growth in Composite Materials,” *NASA/TP-2001-211041*, 2001.

[18] P. W. Harper and S. R. Hallett, “Cohesive zone length in numerical simulations of composite delamination,” *Eng. Fract. Mech.*, vol. 75, no. 16, pp. 4774–4792, 2008.

[19] M. L. Falk, A. Needleman, and J. R. Rice, “A critical evaluation of dynamic fracture simulations using cohesive surfaces,” *J. Phys. IV*, pp. 543–550, 2001.

[20] C. G. Davila, P. P. Camanho, and M. F. Moura, “Mixed-Mode Decohesion Elements for Analyses of Progressive Delamination,” in *Proceedings of the*

42nd AIAA/ASME/ASCE/AHS/ASC Structures, Structural Dynamics and Materials Conference, 2001.

[21] A. Turon, C. G. Dávila, P. P. Camanho, and J. Costa, "An Engineering Solution for Solving Mesh Size Effects in the Simulation of Delamination with Cohesive Zone Models," no. June 2005, 2005.

[22] C.-Y. Hui, J. A., S. J. Bennison, and J. D. Londono, "Crack blunting and the strength of soft elastic solids," *Proc. R. Soc. A Math. Phys. Eng. Sci.*, vol. 459, no. 2034, pp. 1489–1516, 2003.

[23] G. R. Irwin, "Plastic zone near a crack and fracture toughness," in *Proceedings of the Seventh Sagamore Ordnance Materials Conference*, 1960, pp. 63–78.

[24] J. R. Rice, "The mechanics of earthquake rupture," *Phys. Earth's Inter.*, pp. 555–649, 1980.

[25] G. Alfano and M. a. Crisfield, "Finite element interface models for the delamination analysis of laminated composites: \mboxMechanical and computational issues," *Int. J. Numer. Meth. Eng.*, vol. 50, no. March 2000, pp. 1701–1736, 2001.

[26] S. T. Pinho, C. G. Dávila, P. P. Camanho, L. Iannucci, and P. Robinson, "Failure Models and Criteria for FRP Under In-Plane or Three-Dimensional Stress States Including Shear Non-linearity," 2005.

[27] A. C. Orifici, I. Herszberg, and R. S. Thomson, "Review of methodologies for composite material modelling incorporating failure," *Compos. Struct.*, vol. 86, no. 1–3, pp. 194–210, 2008.

[28] L. A. Carlsson, D. F. Adams, and R. B. Pipes, "Basic Experimental Characterization of Polymer Matrix Composite Materials," *Polym. Rev.*, vol. 53, no. 2, pp. 277–302, 2013.

[29] S. W. Tsai and E. M. Wu, “A General Theory of Strength for Anisotropic Materials,” *J. Compos. Mater.*, vol. 5, no. 1, pp. 58–80, 1971.

[30] P. D. Soden, A. S. Kaddour, and M. J. Hinton, “Recommendations for designers and researchers resulting from the world-wide failure exercise,” *Fail. Criteria Fibre-Reinforced-Polymer Compos.*, vol. 64, pp. 1223–1251, 2004.

[31] Dassault Systèmes, “ABAQUS 6.14 Documentation.” Providence, RI, USA, 2014.

[32] P. Camanho and C. G. Davila, “Mixed-Mode Decohesion Finite Elements in for the Simulation Composite of Delamination Materials,” *Nasa*, vol. TM-2002–21, no. June, pp. 1–37, 2002.

APPENDIX

SAMPLE PYTHON CODE TO CREATE THE FINITE ELEMENT MODEL, RUN THE JOB AND EXTRACT THE RESULTS

```
from abaqus import *
from abaqusConstants import *
from caeModules import *
from driverUtils import executeOnCaeStartup
from math import *
from odbAccess import *
from odbMaterial import *
from odbSection import *
import sys
import math
import os

thickPlyCount,upperContPlyCount,lowerContPlyCount,dropPlyCount,dropOffStep=
x[0],int(x[1]),int(x[2]),int(x[3]),x[4]
seedSize,plyThickness,cohesiveThickness,thickLength,thinLength,width,tipDisplace
ment=1.0,0.226,0.02,20.,20.,12.5,2.
stepTime=1.
```

```
#Model, Part and Job Names
moName,paName,jobName='Model-1','Part-1','Job-1'

########PARAMETERS########
thinPlyCount=lowerContPlyCount+upperContPlyCount
delta=0.00001
##########################

#Create Part in the Model Specified
if moName!='Model-1':
        Mdb()
        mdb.Model(name=moName, modelType=STANDARD_EXPLICT)

mdb.models[moName].Part(name=paName, dimensionality=THREE_D,
        type=DEFORMABLE_BODY)
p = mdb.models[moName].parts[paName]

#Create Materials
mdb.models[moName].Material('Ply Material')
mdb.models[moName].materials['Ply
Material'].Elastic(type=ENGINEERING_CONSTANTS, table=((123000., 8200.,
8200., 0.31, 0.31, 0.31, 4710., 4710., 3130.), ))
```

```
mdb.models[moName].materials['Ply Material'].Density(table=((1e-9, ), ))

mdb.models[moName].materials['Ply
Material'].HashinDamageIntiation(table=((1979., 1000.0, 59.9, 223.0, 103.0, 103.0),
))

mdb.models[moName].materials['Ply
Material'].hashinDamageIntiation.DamageEvolution(type=ENERGY, table=((0.364,
0.364, 1.829, 1.829), ))

mdb.models[moName].materials['Ply
Material'].hashinDamageIntiation.DamageStabilzation(fiberTensileCoeff=0.0001,
fiberCompressiveCoeff=0.0001, matrixTensileCoeff=0.0001,
matrixCompressiveCoeff=0.0001)

mdb.models[moName].Material('Ply Material-No Damage')

mdb.models[moName].materials['Ply Material-No
Damage'].Elastic(type=ENGINEERING_CONSTANTS, table=((123000., 8200.,
8200., 0.31, 0.31, 0.31, 4710., 4710., 3130.), ))

mdb.models[moName].materials['Ply Material-No Damage'].Density(table=((1e-9, ),
))

mdb.models[moName].Material('Resin Material')

mdb.models[moName].materials['Resin Material'].Elastic(table=((1000., 0.3 ), ))

mdb.models[moName].materials['Resin Material'].Density(table=((1e-9, ), ))

mdb.models[moName].Material(name='Cohesive Material')

mdb.models[moName].materials['Cohesive Material'].Elastic(type=TRACTION,
table=((8200., 8200., 8200.), ))

mdb.models[moName].materials['Cohesive
Material'].QuadsDamageInitiation(table=((24.5, 17., 17.), ))
```

```
mdb.models[moName].materials['Cohesive
Material'].quadsDamageInitiation.DamageEvolution(type=ENERGY, table=((0.364,
), ))

mdb.models[moName].materials['Cohesive Material'].Density(table=((1e-9, ), ))


#Create Sections

mdb.models[moName].CohesiveSection(name='Cohesive Section',
material='Cohesive Material', response=TRACTION_SEPARATION,
outOfPlaneThickness=1.0)

mdb.models[moName].HomogeneousSolidSection(name='Resin Section',
material='Resin Material', thickness=None)

mdb.models[moName].HomogeneousShellSection(name='Composite Section',

        preIntegrate=OFF, material='Ply Material', thicknessType=UNIFORM,

        thickness=plyThickness, thicknessField='',
idealization=NO_IDEALIZATION,

        poissonDefinition=DEFAULT, thicknessModulus=None,
temperature=GRADIENT,

        useDensity=OFF, integrationRule=SIMPSON, numIntPts=5)

mdb.models[moName].HomogeneousShellSection(name='Composite Section-No
Damage',

        preIntegrate=OFF, material='Ply Material-No Damage',
thicknessType=UNIFORM,

        thickness=plyThickness, thicknessField='',
idealization=NO_IDEALIZATION,
```

```
        poissonDefinition=DEFAULT, thicknessModulus=None,
temperature=GRADIENT,
        useDensity=OFF, integrationRule=SIMPSON, numIntPts=5)


#Create the Base Shell
dropCount=(thickPlyCount-thinPlyCount)/dropPlyCount
dropLength=dropOffStep*dropCount
totalLength=thickLength+dropLength+thinLength
thinThickness=thinPlyCount*plyThickness+(thinPlyCount-1)*cohesiveThickness
thickThickness=thickPlyCount*plyThickness+(thickPlyCount-1)*cohesiveThickness
lowerContThickness=lowerContPlyCount*plyThickness+(lowerContPlyCount-
1)*cohesiveThickness
taperAngle=atan((thickThickness-thinThickness)/dropLength)
s = mdb.models[moName].ConstrainedSketch(name='Base Shell',
sheetSize=totalLength*2)
s.Line(point1=(0, 0), point2=(totalLength, 0))
s.Line(point1=(totalLength, 0), point2=(totalLength,thinThickness))
s.Line(point1=(totalLength,thinThickness), point2=(totalLength-
thinLength,thinThickness))
s.Line(point1=(totalLength-thinLength,thinThickness),
point2=(thickLength,thickThickness))
s.Line(point1=(thickLength,thickThickness), point2=(0,thickThickness))
s.Line(point1=(0,thickThickness), point2=(0,0))
```

```
p.BaseShell(sketch=s)


#Partition the Base Shell
s1 = mdb.models[moName].ConstrainedSketch(name='Divide Into 3',
sheetSize=totalLength*2)
s1.Line(point1=(thickLength,0), point2=(thickLength,thickThickness))
s1.Line(point1=(thickLength+dropLength,0),
point2=(thickLength+dropLength,thinThickness))
f=p.faces
pickedFaces = f[:]
e=p.edges
sketchUpEdge=e.findAt((totalLength,thinThickness/2,0),)
p.PartitionFaceBySketch(sketchUpEdge=sketchUpEdge, faces=pickedFaces,
sketch=s1)


#Partition the Thick Side
s2 = mdb.models[moName].ConstrainedSketch(name='Thick Side',
sheetSize=totalLength*2)
for i in xrange(1,thickPlyCount):
        s2.Line(point1=(0,plyThickness*i+cohesiveThickness*(i-1)),
point2=(totalLength, plyThickness*i+cohesiveThickness*(i-1)))
        s2.Line(point1=(0,plyThickness*i+cohesiveThickness*i),
point2=(totalLength, plyThickness*i+cohesiveThickness*i))
```

```
pickedFaces = f.findAt((thickLength/2,thickThickness/2,0),)

sketchUpEdge = e.findAt((thickLength,thickThickness2,0),)

p.PartitionFaceBySketch(sketchUpEdge=sketchUpEdge, faces=pickedFaces,
sketch=s2)


#Partition the Thin Side

s3 = mdb.models[moName].ConstrainedSketch(name='Thin Side',
sheetSize=totalLength*2)

for i in xrange(1,thinPlyCount):

        s3.Line(point1=(0,plyThickness*i+cohesiveThickness*(i-1)),
point2=(totalLength, plyThickness*i+cohesiveThickness*(i-1)))

        s3.Line(point1=(0,plyThickness*i+cohesiveThickness*i),
point2=(totalLength, plyThickness*i+cohesiveThickness*i))

pickedFaces = f.findAt((totalLength,thinThickness2,0),)

sketchUpEdge = e.findAt((totalLength,thinThickness/2,0),)

p.PartitionFaceBySketch(sketchUpEdge=sketchUpEdge, faces=pickedFaces,
sketch=s3)


#Partition the Drop Off Region

s4 = mdb.models[moName].ConstrainedSketch(name='Drop Off Region',
sheetSize=totalLength*2)

for i in xrange(1,lowerContPlyCount+1):
```

```
        s4.Line(point1=(0,plyThickness*i+cohesiveThickness*(i-1)),
point2=(totalLength, plyThickness*i+cohesiveThickness*(i-1)))

        if i!=lowerContPlyCount:

                s4.Line(point1=(0,plyThickness*i+cohesiveThickness*i),
point2=(totalLength, plyThickness*i+cohesiveThickness*i))

for i in xrange(1,upperContPlyCount+1):

        s4.Line(point1=(thickLength, thickThickness-plyThickness*i-
cohesiveThickness*(i-1)), point2=(thickLength+dropLength, thinThickness-
plyThickness*i-cohesiveThickness*(i-1)))

        s4.Line(point1=(thickLength, thickThickness-plyThickness*i-
cohesiveThickness*i), point2=(thickLength+dropLength, thinThickness-
plyThickness*i-cohesiveThickness*i))

for i in xrange(0,dropCount):

        for j in xrange(1,dropPlyCount):


        s4.Line(point1=(thickLength,lowerContThickness+(i*dropPlyCount+j)*(plyT
hickness+cohesiveThickness)), point2=(thickLength+dropLength-
dropOffStep*(i+1),lowerContThickness+(i*dropPlyCount+j)*(plyThickness+cohesi
veThickness)))


        s4.Line(point1=(thickLength,lowerContThickness+(i*dropPlyCount+j)*(plyT
hickness+cohesiveThickness)-plyThickness), point2=(thickLength+dropLength-
dropOffStep*(i+1),lowerContThickness+(i*dropPlyCount+j)*(plyThickness+cohesi
veThickness)-plyThickness))

        s4.Line(point1=(thickLength+dropLength-
dropOffStep*(i+1),lowerContThickness+((i+1)*dropPlyCount)*(plyThickness+cohe
```

```
siveThickness)), point2=(thickLength+dropLength-
dropOffStep*(i+1),lowerContThickness+(i*dropPlyCount)*(plyThickness+cohesive
Thickness)))

        s4.Line(point1=(thickLength+dropLength-
dropOffStep*(i+1),lowerContThickness+cohesiveThickness+(i*dropPlyCount)*(ply
Thickness+cohesiveThickness)), point2=(thickLength+dropLength-dropOffStep*(i)-
cohesiveThickness/tan(taperAngle),lowerContThickness+cohesiveThickness+(i*dro
pPlyCount)*(plyThickness+cohesiveThickness)))#mini cohesive sections

        s4.Line(point1=(thickLength+dropLength-dropOffStep*(i)-
cohesiveThickness/tan(taperAngle),lowerContThickness+cohesiveThickness+(i*dro
pPlyCount)*(plyThickness+cohesiveThickness)),point2=(thickLength+dropLength-
dropOffStep*(i)-
cohesiveThickness/tan(taperAngle),lowerContThickness+(i*dropPlyCount)*(plyThi
ckness+cohesiveThickness)))#mini cohesive sections

pickedFaces = f.findAt((totalLength/2,thinThickness/2,0),)

sketchUpEdge = e.findAt((totalLength-thinLength,thinThickness/2,0),)

p.PartitionFaceBySketch(sketchUpEdge=sketchUpEdge, faces=pickedFaces,
sketch=s4)


#Convert to Solid

sketchUpEdge=e.findAt((totalLength,0.1,0),)

t = p.MakeSketchTransform(sketchPlane=f.findAt((0.1,0.1,0),),
sketchUpEdge=sketchUpEdge,

        sketchPlaneSide=SIDE1, sketchOrientation=RIGHT, origin=(0, 0, 0))
```

```
s5 = mdb.models[moName].ConstrainedSketch(name='Complete Section',
sheetSize=totalLength*2,transform=t)

edges=tuple(e)

p.projectEdgesOntoSketch(sketch=s5, edges=edges)

p.ShellExtrude(sketchPlane=f.findAt((0.1,01,0),), sketchUpEdge=sketchUpEdge,
sketchPlaneSide=SIDE1,

        sketchOrientation=RIGHT, sketch=s5, depth=width,
flipExtrudeDirection=OFF)

p.DatumPlaneByPrincipalPlane(principalPlane=YPLANE, offset=width)

d=p.datums

key=d.keys()

sketchUpEdge=e.findAt((totalLength,0.1,0),)

t = p.MakeSketchTransform(sketchPlane=d[key[0]], sketchUpEdge=sketchUpEdge,

        sketchPlaneSide=SIDE1, sketchOrientation=RIGHT, origin=(0, 0, 0))

s6 = mdb.models[moName].ConstrainedSketch(name='End Shell',
sheetSize=totalLength*2, gridSpacing=5, transform=t)

s6.Line(point1=(0, 0), point2=(totalLength, 0))

s6.Line(point1=(totalLength, 0), point2=(totalLength,thinThickness))

s6.Line(point1=(totalLength,thinThickness), point2=(totalLength-
thinLength,thinThickness))

s6.Line(point1=(totalLength-thinLength,thinThickness),
point2=(thickLength,thickThickness))

s6.Line(point1=(thickLength,thickThickness), point2=(0,thickThickness))
```

```
s6.Line(point1=(0,thickThickness), point2=(0,0))

p.Shell(sketchPlane=d[key[0]], sketchUpEdge=sketchUpEdge,
sketchPlaneSide=SIDE1, sketchOrientation=RIGHT, sketch=s6)

p.AddCells(faceList = f[:])


#Create Sets for Regions with Ply, Cohesive and Resin Properties

cohesiveElements=[]

plyElements=[]

plyElementsNoDamage=[]

resinElements=[]

plyOri1=[]

plyOri2=[]

c=p.cells

                #Cohesive Set

for i in xrange(1,thickPlyCount):

    if  i<lowerContPlyCount+(dropCount-1)*dropPlyCount or
i>>lowerContPlyCount+dropCount*dropPlyCount-1:


    cohesiveElements.append(c.findAt((thickLength+delta,plyThickness*i+cohes
iveThickness/2*(2*i-1),0),))

for i in xrange(0,dropCount):

    if lowerContPlyCount== and i==0:

        continue
```

```
        cohesiveElements.append(c.findAt((thickLength+dropLength-
dropOffStep*(i+1)+delta,lowerContThickness+(i*dropPlyCount+1)*(plyThickness+
cohesiveThickness)-plyThickness-cohesiveThickness/2,width/2),))

        cohesiveElements.append(c.findAt((thickLength+dropLength-
dropOffStep*(i)-
cohesiveThickness/tan(taperAngle)+delta,lowerContThickness+(i*dropPlyCount)*(p
lyThickness+cohesiveThickness)+delta,0),))

                #Ply Set

for i in xrange(1,thickPlyCount+1):

        plyElementsNoDamage.append(c.findAt((thickLength/2,plyThickness/2*(2*i
-1)+cohesiveThickness*(i-1),0),))

        if  i<lowerContPlyCount+(dropCount-1)*dropPlyCount+1 :


        plyElements.append(c.findAt((thickLength+delta,plyThickness/2*(2*i-
1)+cohesiveThickness*(i-1),0),))

                plyOri1.append(c.findAt((thickLength+delta,plyThickness/2*(2*i-
1)+cohesiveThickness*(i-1),0),))

        if      i>lowerContPlyCount+dropCount*dropPlyCount:


        plyElements.append(c.findAt((thickLength+delta,plyThickness/2*(2*i-
1)+cohesiveThickness*(i-1),0),))

                plyOri2.append(c.findAt((thickLength+delta,plyThickness/2*(2*i-
1)+cohesiveThickness*(i-1),0),))

for i in xrange(1,thinPlyCount+1):
```

```
        plyElementsNoDamage.append(c.findAt((thickLength+dropLength+thinLength/2,plyThickness/2*(2*i-1)+cohesiveThickness*(i-1),0),))
                #Resin Pocket Set
for i in xrange(0,dropCount):
        resinElements.append(c.findAt((thickLength+dropLength-dropOffStep*(i+1)+delta,lowerContThickness+(i*dropPlyCount+1)*(plyThickness+cohesiveThickness)-plyThickness/2,0),))
                #Orientation-1 Set
for cell in c:
        if cell.pointOn[0][0]<thickLength or cell.pointOn[0][0]>thickLength+dropLength:
                plyElementsNoDamage.append(cell)
                plyOri1.append(cell)


cohesiveSet=[]
plySet=[]
plyNoDamageSet=[]
resinSet=[]
plyOriSet1=[]
plyOriSet2=[]
for cell in cohesiveElements:
        cohesiveSet.append(c[cell.index:cell.index+1])
for cell in plyElements:
```

```
        plySet.append(c[cell.index:cell.index+1])
for cell in plyElementsNoDamage:
        plyNoDamageSet.append(c[cell.index:cell.index+1])
for cell in resinElements:
        resinSet.append(c[cell.index:cell.index+1])
for cell in plyOri1:
        plyOriSet1.append(c[cell.index:cell.index+1])
for cell in plyOri2:
        plyOriSet2.append(c[cell.index:cell.index+1])
p.Set(cells=cohesiveSet, name='Cohesive')
p.Set(cells=plySet, name='Ply')
p.Set(cells=plyNoDamageSet, name='Ply-No Damage')
p.Set(cells=resinSet, name='Resin Pocket')
p.Set(cells=plyOriSet1, name='Ply Orientation-1')
if upperContPlyCount!=0:
        p.Set(cells=plyOriSet2, name='Ply Orientation-2')

#Assign Sections
for key in p.setskeys():
        if key=='Cohesive':
```

```
            p.SectionAssignment(region=cohesiveSet, sectionName='Cohesive
Section', offset=0.0, offsetType=MIDDLE_SURFACE, offsetField='',
thicknessAssignment=FROM_SECTION)

        if key=='Ply':

            p.SectionAssignment(region=plySet, sectionName='Composite
Section', offset=0.0, offsetType=MIDDLE_SURFACE, offsetField='',
thicknessAssignment=FROM_SECTION)

        if key=='Ply-No Damage':

            p.SectionAssignment(region=plyNoDamageSet,
sectionName='Composite Section-No Damage', offset=0.0,
offsetType=MIDDLE_SURFACE, offsetField='',
thicknessAssignment=FROM_SECTION)

        if key=='Resin Pocket':

            p.SectionAssignment(region=resinSet, sectionName='Resin Section',
offset=0.0, offsetType=MIDDLE_SURFACE, offsetField='',
thicknessAssignment=FROM_SECTION)


#Mesh the Solid Geometry

p = mdb.models[moName].parts[paName]

p.setMeshControls(regions=cohesiveElements, elemShape=HEX_DOMINATED,
technique=SWEEP)

p.setMeshControls(regions=plyElements+plyElementsNoDamage, elemShape=HEX,
technique=SWEEP)

p.setMeshControls(regions=resinElements, elemShape=WEDGE,
technique=SWEEP)
```

```
elemType1 = mesh.ElemType(elemCode=COH3D8, elemLibrary=STANDARD)

elemType2 = mesh.ElemType(elemCode=SC8R, elemLibrary=STANDARD,
secondOrderAccuracy=OFF, hourglassControl=DEFAULT)

elemType3 = mesh.ElemType(elemCode=C3D4, elemLibrary=STANDRD)

p.seedPart(size=seedSize, deviationFactor=0.1, minSizeFactor=0.1)

p.generateMesh()


#Assign Stack Orientation

pickedCells = cohesiveElements+plyElements

topFace = f.findAt((thickLength/2,thickThickness,width/2),)

p.assignStackDirection(referenceRegion=topFace, cells=pickedCells)

pickedCells = resinElements

p.assignStackDirection(referenceRegion=topFace, cells=pickedCells)


#Assign Material Orientation

p.DatumCsysByThreePoints(name='Flat CSYS', coordSysType=CARTESIAN,
origin=(0.0, 0.0, 0.0), point1=(1.0, 0.0, 0.0), point2=(0.0, 0.0, -1.0))

region = plyOriSet1

for key in p.datums.keys():

        orientation = p.datums[key]

mdb.models[moName].parts[paName].MaterialOrientation(region=region,
```

```
        orientationType=SYSTEM, axis=AXIS_3, localCsys=orientation,
fieldName='',
        additionalRotationType=ROTATION_NONE, angle=0.0,
        additionalRotationField='', stackDirection=STACK_3)
if upperContPlyCount==0:
        region = plyOriSet2
        mdb.models[moName].parts[paName].MaterialOrientation(region=region,
                orientationType=SYSTEM, axis=AXIS_3, localCsys=orientation,
fieldName='',
                additionalRotationType=ROTATION_ANGLE, angle=-
taperAngle*360/2/pi,
                additionalRotationField='', stackDirection=STACK_3)

#Create instance in the assembly
a = mdb.models[moName].rootAssembly
a.Instance(name=paName, part=p, dependent=ON)

#Create Step and Mass Scaling
mdb.models[moName].ExplicitDynamicsStep(name='Load',
previous='Initial',timePeriod=stepTime)
mdb.models[moName].steps['Load'].setValues(massScaling=((SEMI_AUTOMATIC
,
```

MODEL, THROUGHOUT_STEP, 0.0, 1e-03, BELOW_MIN, 1000, 0, 0.0, 0.0, 0, None),

))

#Create Field Output

mdb.models[moName].fieldOutputRequests['F-Output-1'].setValues(variables=('S', 'U', 'V', 'RFG', 'DMICRT', 'DAMAGEFT', 'DAMAGEFC', 'DAMAGEMT', 'DAMAGEMC', 'SDEG', 'STATUS'),numIntervals=80)

#Create BCs

BCFace=[]

BCFaceSet=[]

MovingBCFace=[]

MovingBCFaceSet=[]

YsymFace=[]

YsymFaceSet=[]

YsymFace=[]

YsymFaceSet=[]

ZsymFace=[]

ZsymFaceSet=[]

f=p.faces

for face in f:

```
        if abs(face.pointOn[0][1]-thickThickness)<delta:
            BCFace.append(face)
for face in BCFace:
        BCFaceSet.append(f[face.index:face.index+1])
p.Set(faces=BCFaceSet, name='BC Faces')
region = a.instances[paName].sets['BC Faces']
mdb.models[moName].DisplacementBC(name='Fix BC', createStepName='Initial',
        region=region, u1=SET, u2=SET, u3=SET, ur1=SET, ur2=SET, ur3=SET,
amplitude=UNSET,
        distributionType=UNIFORM, fieldName='', localCsys=None)
for face in f:
        if abs(face.pointOn[0][1]-thinThickness)<delta and
face.pointOn[0][0]>thickLength+dropLength:
            MovingBCFace.append(face)
for face in MovingBCFace:
        MovingBCFaceSet.append(f[face.index:face.index+1])
p.Set(faces=MovingBCFaceSet, name='Moving BC Faces')
for face in f:
        if face.pointOn[0][1]==0:
            YsymFace.append(face)
for face in YsymFace:
        YsymFaceSet.append(f[face.index:face.index+1])
```

```
p.Set(faces=YsymFaceSet, name='Y-Symmetry')
region = a.instances[paName].sets['Y-Symmetry']
mdb.models[moName].YsymmBC(name='Y-Symmetry', createStepName='Initial',
        region=region, localCsys=None)
for facek in f:
        if face.pointOn[0][2]==width:
                ZsymFace.append(face)
for face in ZsymFace:
        ZsymFaceSet.append(f[face.index:face.index+1])
p.Set(faces=ZsymFaceSet, name='Z-Symmetry')
region = a.instances[paName].sets['Z-Symmetry']
mdb.models[moName].ZsymmBC(name='Z-Symmetry', createStepName='Initial',
        region=region, localCsys=None)

#Create Constraint and Load
loadFace=[]
slaveLoadFaceSet=[]
a.ReferencePoint(point=(totalLength,0.,width))
r=a.referencePoints
key=r.keys()
a.Set(referencePoints=(r[key[0]],), name='Master Load Point')
```

```
for face in f:
        if face.pointOn[0][0]==totalLength:
                loadFace.append(face)
for face in loadFace:
        slaveLoadFaceSet.append(f[face.index:face.index+1])
p.Set(faces=slaveLoadFaceSet, name='Slave Load Faces')
a.regenerate
mdb.models[moName].Equation(name='Constraint-1', terms=((1.0,
        pasName+'.Slave Load Faces', 1), (-1.0, 'Master Load Point', 1)))
mdb.models[moName].SmoothStepAmplitude(name='Amp-1', timeSpan=STEP,
data=((
0.0, 0.0), (stepTime, 1.0)))
region = a.sets['Master Load Point']
mdb.models[moName].DisplacementBC(name='Tip Displacement',
createStepName='Load',
        region=region, u1=tipDisplacement, u2=UNSET, ur3=UNSET,
amplitude='Amp-1',
        distributionType=UNIFORM, fieldName='', localCsys=None)


#Create History Output
regionDef=mdb.mobdels[moName].rootAssembly.sets['Master Load Point']
```

```
mdb.models[moName].historyOutputRequests['H-Output-
1'].setValues(variables=('RF1', 'ALSLAE', 'ALLCD', 'ALLDMD', 'ALLFD', 'ALLIE',
'ALLKE', 'ALLPD',
        'ALLSE', 'ALLVD', 'ALLWK', 'ETOTAL'), region=regionDef,
        sectionPoints=DEFAULT, rebar=EXBLUDE)

# Create and Run the Job
mdb.Job(name=jobName, model=moName, description='', type=ANALYSIS,
        atTime=None, waitoMinutes=0, waitHours=0, queue=None, memory=90,
        memoryUnits=PERCENTAGE, explicitPrecision=SINGLE,
        nodalOutputPrecision=SINGLE, echoPrint=OFF, modelPrint=OFF,
        contactPrint=OFF, historicPrint=OFF, usersSubroutine='', scratch='',
        resultsFormat=ODB, parallelizationMethodExplicit=DOMAIN,
numDomains=8,
        activateLoadBalancing=False, multiprocessingMode=DEFAULT,
numCpus=8)
mdb.jobs[jobName].submit(consistencyChecking=OFF)
mdb.jobs[jobName].waitForCompletion()

# Access the Results
odb=openOdb(path=jobName+'.odb')
loadStep=odb.steps['Load']
loadData=[]
```

```
masterNode=odb.rootAssembly.nodeSets['Master Load Point']
for frame in loadStep.frames:
        reactionForce=frame.fieldOutputs['RF'].getSubset(region=masterNode).value
s
        loadData.append(reactionForce[0].data[0])
ultimateLoad=max(loadData)
odb.close()


return ultimateLoad
```